Full length article

The transformation matrix in the 7DOFs beam formulation

Claudio Bernuzzi, Marco Simoncelli *

Department of Architecture, Built Environment and Construction Engineering, Politecnico di Milano, Italy

A R T I C L E   I N F O

A B S T R A C T

A non-negligible percentage of steel products for civil and industrial constructions is realised with members characterised by a mono-symmetric cross-section. The non-coincidence between the centroid and the shear centre reflects in a quite complex behaviour that is remarkably influenced by the warping effects. Usually, frame design is based on the output data of commercial Finite Element Analysis Packages (FEAPs) but only few of them offer a refined beam element formulation able to reproduce the response of non-bisymmetric cross-section members (like the 7 degrees of freedom, DOFs, beam element). As a consequence, warping effects are usually neglected in routine design, leading in several cases to assess non-correct internal stresses, global displacements and critical buckling multipliers.

This paper is focussed on mono-symmetric cross-section members and deals with the influence of the interaction between axial force, bending moments and bimoment in linear elastic range. In particular, the two strategies that FE developers usually adopt, in the 7 DOFs beam formulation, to pass from the local to the global reference system are herein shortly introduced and discussed. The effects of the associated transformation matrices have been investigated in few examples, also reproduced via closed expressions derived from the mixed torsion theory and FE shell models. Paper outcomes show that the results in terms of generalised displacements, internal forces and, consequently, stress distribution along the member cross-section are significantly different, strictly depending on the adopted transformation matrix. The importance of a correct evaluation of the bimoment distribution is stressed also by the fact that the new edition of the EN1993-1-1, expected in the next months, includes also the bimoment contribution for member checks.

1. Introduction

The design of steel frames is generally carried out by using commercial finite element analysis packages (FEAPs) offering *beam* elements whose formulation efficiently represents the response of members having two axes of symmetry. For each node 6 degree of freedoms (DOFs) are generally considered, as showed in Fig. 1a. Reference is made to three displacements (u, v and δ) and three rotations (φ_x, φ_y and φ_z) and to the associated generalised forces, i.e. axial force (N), shear forces (F_y and F_z), bending moments (M_y and M_z) and the torsional moment (M_x). It is worth noting that in steel construction practice mono-symmetric cross-section members are quite frequently used, not only for isolated components, like purlins and wall girts, but also for several types of structures such as lifting equipment systems (tower cranes, derricks, etc.) as well as for industrial steel storage racks. The formers are generally composed of built-up compressed members with hot-rolled angles [1], whereas the latter have a skeleton frame realised via cold-formed cross-section elements [2]. Due to the absence of two axes of symmetry, the cross-section centroid (point O) generally does not coincide with the shear centre (point S). As a consequence, the quite complex structural behaviour is significantly influenced by the interactions between bending moments and warping torsion [3–6], that cannot be captured via the previously introduced 6 degrees of freedom (DOFs) *beam* formulation. To simulate the correct behaviour of these cross-sections, more refined FE *beam* formulations able to account for warping torsion are necessary. These formulations are available in literature since few decades, considering also plasticity and large displacements [7–12]. As an example, Addessi et al. [13] presented three different *beam* FE formulations based on different kinematic assumptions to describe the out-of-plane cross-section deformations. In particular, in the third proposed model, warping has been described by introducing additional degrees of freedom on the cross-section plane, making hence possible an accurate description of the out-of-plane deformations. In all the validation examples discussed in the previously mentioned references, only the interactions between bimoment and shear forces or torsion have been considered. No attention has been paid on the axial-force bimoment interaction. Furthermore, another proposed *beam* element, whose formulation is based on the Generalised Beam Theory (GBT) [14], incorporates a great number of sectional degrees of freedom allowing for capturing

SYMBOLS

Greek lower-case symbol

α	angle between local and principal axes
α_{cr}	critical load multiplier
δ	vertical displacement
δ_F	vertical displacement due to the flexure
δ_w	vertical displacement due to the bimoment
θ	warping
λ_T	torsional slenderness
v	Poisson ratio
ρ	radius
σ	normal stress
σ_F	normal stress due to the flexure
σ_w	normal stress due to the bimoment
φ_{ip}	particular solution
φ_x	rotation about x-axis
φ_y	rotation about y-axis
φ_z	rotation about z-axis
ω	sectorial area
ω_{mean}	mean sectorial area
ω_o	sectorial area with respect to the centroid
$\omega_{s,max}$	maximum normalized sectorial area
ω_s	sectorial area with respect to the shear centre

Latin lower-case symbol

a, g	distances defined in Figs. 5 and 7
b, b_1, b_2	flanges length
b_s, h_s	distance of shear centre from the global axes
d*	dimensionless displacement
h	web height
i, k	generic points
j, p	nodal points
s	abscissa
t	thickness
u	axial displacement
$\{u\}$	vector of the displacements
v	lateral displacement
v_F	lateral displacement due to bending
v_w	lateral displacement due to bimoment
x, y, z	local axes
y_0, z_0	co-ordinates of the centroid
y_s, z_s	distance between shear centre and centroid

Latin upper-case symbol

A, D	points of the cross-section
A_g	cross-section area
B	bimoment
C1, C2, C3	constants of integration
E	Young modulus
F_y	shear force in y-axis
F_z	shear force in z-axis
$\{F\}$	vector of the forces
F*	nondimensional force
G	tangential modulus
I_w	warping constant
I_y	second moment of area with respect the y-axis
I_z	second moment of area with respect the z-axis
I_t	torsional constant

|	
$[K]^{E,l}$	elastic stiffness matrix in the local system
$[K]^{E,g}$	elastic stiffness matrix in the global system
L	length
M_t	uniform (primary) torsional moment
M_x	torsional moment
M_y	bending moment about y-direction
M_z	bending moment about z-direction
M_ω	non uniform (warping) torsional moment
M	bending moment
N	axial force
O	position of the centroid
$\underline{O}$	position of the centroid
$\overline{P}$	external longitudinal force
S	position of the shear centre
$[T]$	transformation matrix
X, Y, Z	global axes
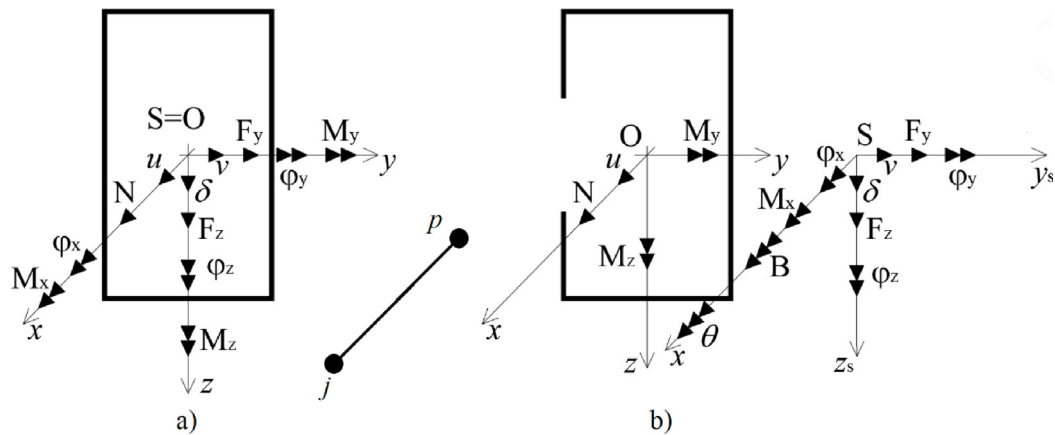
Fig. 1. Nodal displacements and generalised forces for (a) 6DOFs and (b) 7DOFs FE *beam* formulation.

both local and distortional cross-section deformations. The use of GBT elements to model a whole frame can represent a challenge for structural engineers (especially for the modelling of joints) which generally are familiar with more classic FE strategies.

Despite refined approaches are available in literature, only a limited number of commercial FEAPs [15–20] offer *beam* elements accounting for warping. The most common *beam* element in FEAPs is the one having 7 DOFs for each node, in which the seventh DOF is necessary to describe the warping of the cross-section, θ. Warping is defined as the first derivate of the torsional rotation φ_x:

$$\theta(x) = -\frac{d\varphi_x(x)}{dx}$$
(1)

Considering Fig. 1b, reference can be made to the shear centre (S) for the definition of all the generalised displacements, with the exception of the axial displacement u, which is defined in correspondence to the centroid (O). Furthermore, the shear forces (F_y and F_z), the torsional moment (M_x) and the bimoment (B) are referred to S, whereas both bending moments (M_y and M_z) and the axial force (N) are defined with respect to O.

The focus of the paper is to discuss, with the use of 7DOF *beam* element, about the interaction between axial force, bending moments and bimoment in linear elastic range. No attention is herein paid to the problem of the bimoment-axial force interaction for the global stability [21]. In particular, a short introduction related to the thin-walled beam theory is proposed by focussing attention on the sole aspects of relevance for the study. Furthermore, the two transform matrices usually adopted with the 7 DOFs element, to pass from the local to the global reference system are shortly presented and discussed. Both have been implemented in an open FE software for academic use and applied to basic cases, which have been reproduced also by means of the mixed torsion theory [4] and FE *shell* models. A direct comparison between the associated results shows that these transformation matrices are not always equivalent in terms of generalised forces and displacements and, as a consequence, routine design based on one or the other choice could be characterised by different reliability levels.

2. Essential theoretical background

The behaviour of thin-walled members has already been deeply investigated in literature [4,6] but few essential concepts are herein briefly recalled allowing for a better understanding of the paper contents. In particular, the concept of the sectorial area and the two Vlasov's theorems are herein discussed, whose impact is usually ignored in routine design.

The sectorial area. The analysis of thin-walled elements is based on the definition of a suitable geometrical function, $\omega(s)$, that is the cross-section sectorial area. It corresponds to twice the swept area (dashed background in Fig. 2) described by the radius ρ, which moves along the
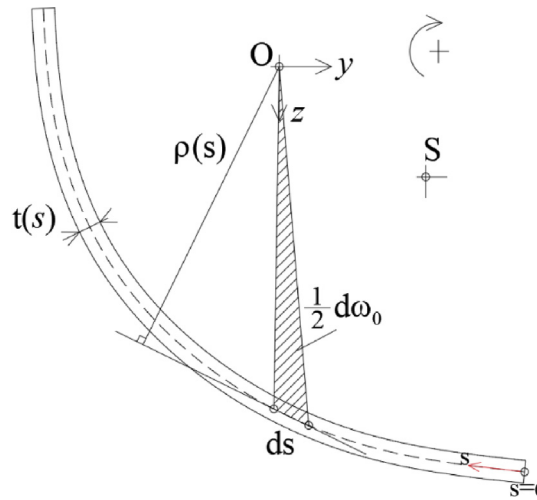
Fig. 2. General definition of the sectorial area (ω).

midline of the cross-section from the point $s = 0$ to the point of interest. The swept area is generally considered positive when radius ρ rotates in the clockwise direction.

When the sectorial area $\omega(s)$ is evaluated with respect to the centroid (O) of the cross-section, it is identified as $\omega_0(s)$ and it can be evaluated (Fig. 2) as:

$$\mathrm{d}\omega_0(s) = \mathrm{d}\omega_0(y, z) = y\,dz - z\,dy = \rho(s)ds \tag{2a}$$

$$\omega_0 = \int_0^s \mathrm{d}\omega_0(s) = \int_0^s \rho(s)ds \tag{2b}$$

Generally, reference is made to the so-called normalised sectorial area, $\omega_s(y, z)$ i.e. the sectorial area evaluated with respect to the shear centre, which can be obtained from equation:

$$\omega_s(y, z) = \omega_0(y, z) + z_s(y - y_0) - y_s(z - z_0) - \omega_{mean} \tag{3}$$

where the position of the centroid (O) and of the shear centre (S) are defined by the couples of co-ordinates (y_0, z_0) and (y_s, z_s), respectively. Term ω_{mean} is a constant value obtained as the average value of ω_o considering its effective distribution along the whole cross-section.

As shown in Fig. 1(b), a key feature of this theory is represented by the presence of an additional generalised internal force that is the bimoment, $B(x)$, obtained as:

$$B(x) = -EI_w \frac{d\theta(x)}{dx} = -EI_w \frac{d^2\varphi(x)}{dx^2} \tag{4}$$

where I_w is second moment of area of the sectorial area (or warping constant) of the whole cross-section, defined as:

$$I_w = \int \omega_s^2 dA_g \tag{5}$$

where A_g is the cross-section area. Once the sectorial area and the warping constant have been appraised, it is possible to define the distribution of the warping normal stress $\sigma_w(x, y, z)$ on the basis of the bimoment value via the equation:

$$\sigma_w(x, y, z) = \frac{B(x)}{I_w} \omega_s(y, z) \tag{6}$$

It is worth noting that the presence of the bimoment is generally ignored in the routine design, because it is not adequately considered in the actual version of the standard provisions [22,23]. Consequently, the most adopted FEAPs do not offer an accurate *beam* formulation and the member safety index is independent of the effective warping stress distribution acting on the cross-section. Moreover, in the future edition of the EN1993-1-1 [24], which is expected to be available in the next months, the bimoment presence will be explicitly considered in the verification equations. As a consequence, its correct evaluation is of paramount importance in order to guarantee a safe design.

Bimoment associated with the axial force. Vlasov [4] investigated the effect of an external applied force, P at a certain point k (y_k, z_k), as showed in Fig. 3, in terms of resulting axial force (N), bending moments (M_y and M_z) and bimoment (B) applied on the cross-section, via the following equations:

$$\begin{cases} N = P \\ M_y = Pz_k \\ M_z = -Py_k \\ B = P\omega_s(y_k, z_k) \end{cases} \tag{7a–d}$$

It is worth noting that the longitudinal force, that is eccentric with respect to the centroid, generates bending moments and bimoment on the cross-section depending on the sectorial area distribution. Eq. (7d) is generally identified as the first Vlasov's theorem, which expresses a direct relationship between the axial force and the bimoment.
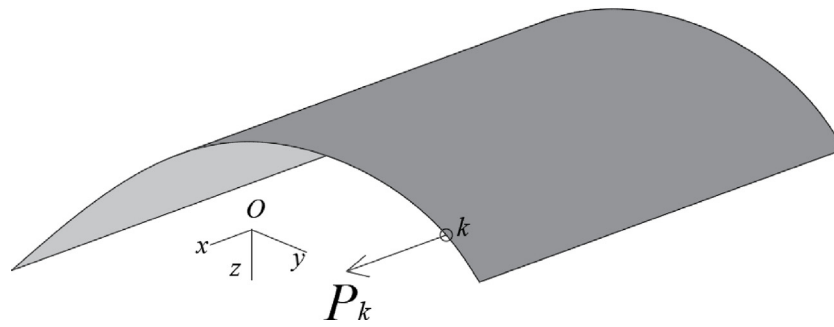
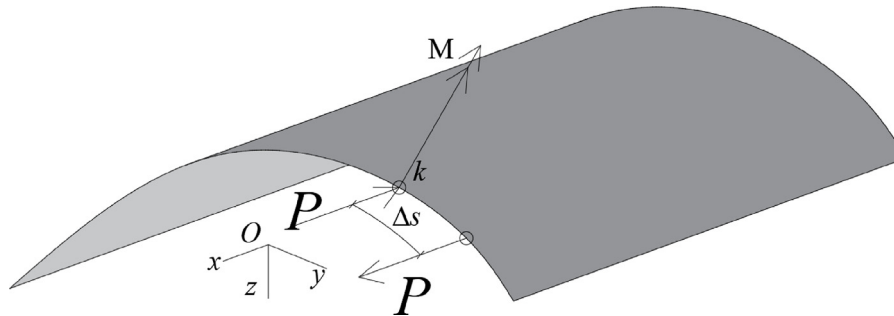**Fig. 3.** Member end loaded by a force P, acting on point k.

Fig. 4. Bending moment acting on the plane of the membrane.

Moreover, by combining Eqs. (7d) and (3), it is possible to express the bimoment as depending on the axial force and bending moments [25].

$$B = P\omega_s(y_k, z_k) = P[\omega_0(y_k, z_k) + z_s(y - y_k) - y_s(z - z_k) - \omega_{mean}] \tag{8a}$$

$$B = P(\omega_{0,k} - \omega_{mean}) + M_z z_S - M_y y_S \tag{8b}$$

Bimoment associated with bending moments. In his second theorem, Vlasov investigated the dependence between bimoment and bending moments. A bending moment, M, acting on the plane tangent to the cross-section in point k can be seen as due to a longitudinal couple of notional forces P, at a certain distance Δs (Fig. 4), ie:

$$M = P\Delta s \tag{9}$$

Starting from Eq. (7d), it is in fact possible to evaluate B as:

$$B = -P\omega_{s,k} + P(\omega_{s,k} + \Delta\omega_{s,k}) = P\Delta\omega_{s,k} \tag{10}$$

From Eq. (10), letting $\Delta s \to 0$, it is possible to obtain the relationship:

$$B = P\Delta\omega_{s,k} = M\left(\frac{\Delta\omega_{s,k}}{\Delta s}\right)_{\Delta s \to 0} = M\left(\frac{d\omega_s}{ds}\right) \tag{11}$$

The bimoment is hence proportional to the value of the first derivate of the sectorial coordinate with respect to the abscissa s and to the applied bending moment.

For a better understanding of the impact of Vlasov's two theorems on the routine design, two practical cases are discussed below.

2.1. Plain channel members

Consider a mono-symmetric plain channel having a constant thickness (t), with h and b representing the height web and the flange width, respectively. For this cross-section, the distributions of ω_0, ω_s and $d\omega_s/ds$ are reported in Fig. 5 together with the value of ω_{mean}.

Considering Vlasov's theorems, if a couple of forces is applied on points D and D' (at a distance equal to h, Fig. 6a), which generates a bending moment M_y, the bimoment can be evaluated by considering three different possibilities, leading to the same results:

(1) in accordance with Eq. (7d), the bimoment value is:

$$B = P\omega_{s,D} + P\omega_{s,D'} = Pg\frac{h}{2} - P(-g\frac{h}{2}) = P\,gh \tag{12a}$$

(2) by considering Eq. (8), it should be noted that the shear centre position y_S is equal to $(g+a)$, whereas term z_S is nil. Bimoment is hence equal to:

$$B = \left[-P\left(-\frac{bh}{2}\right) + P\left(-\frac{bh}{2} - ah\right)\right] + [Ph(g+a)] - \left[P\frac{h}{2}(a+b) - P\frac{h}{2}(a+b)\right] = P\,h\,g \tag{12b}$$

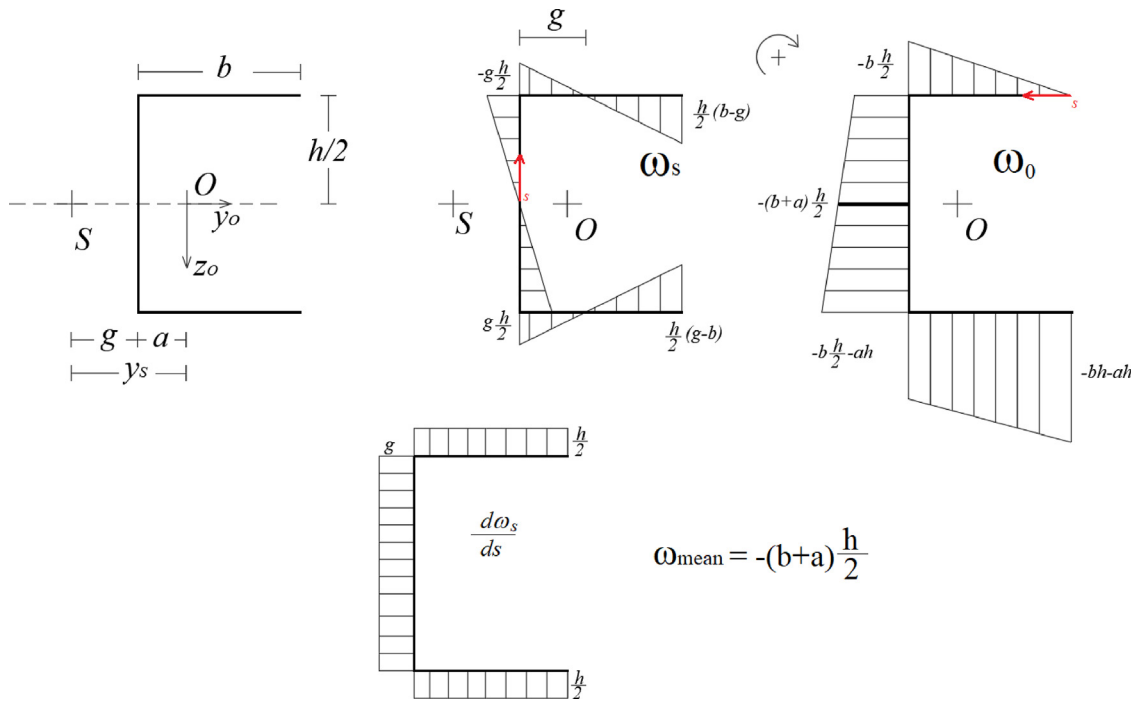**Fig. 5.** Distribution of ω_0, ω_s and $d\omega_s/ds$ for a plain channel.
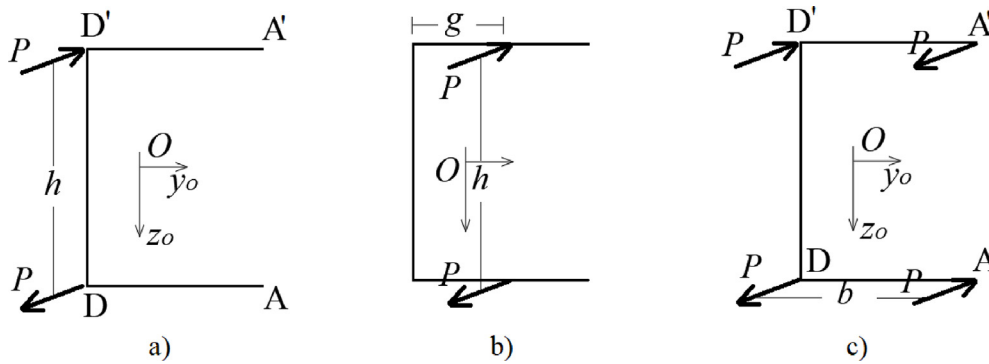

Fig. 6. Different cases of longitudinal forces on a plain channel.

(3) by considering Eq. (11), the bimoment can be related to the derivate of the sectorial area, which is equal to g:

$$B = M\left(\frac{d\omega_s}{ds}\right) = Ph\,g \tag{12c}$$

Two other cases of practical interest are depicted in parts (b) and (c) of Fig. 6. It is especially worth noting that:

- a couple of forces (P) applied in the points where the normalised sectorial area is nil (i.e. at a distance g from the web, Fig. 6b) leads to $B = 0$;
- a system of self-balanced forces (P) generates two opposite moments in the plane of the flanges (in Fig. 6c) and, consequently, $B = Ph\,b$.

2.2. H-shaped members with unequal flanges

Let us consider a H-shaped cross-section having a constant thickness (t), a total height equal to h and different width of the flanges b_1 and b_2. The distributions of ω_0, ω_s and $d\omega_s/ds$ are displayed in Fig. 7, together with ω_{mean}.

A couple of forces applied on points D and D' (at a distance b_1, Fig. 8a) generating a bending moment M_z, leads to a bimoment that can be appraised via different strategies, leading to the same results:

(1) in accordance with Eq. (7d):

$$B = P\omega_{s,D'} + P\omega_{s,D} = Pa\frac{b_1}{2} - P\left(-a\frac{b_1}{2}\right) = P\,ab_1 \tag{13a}$$
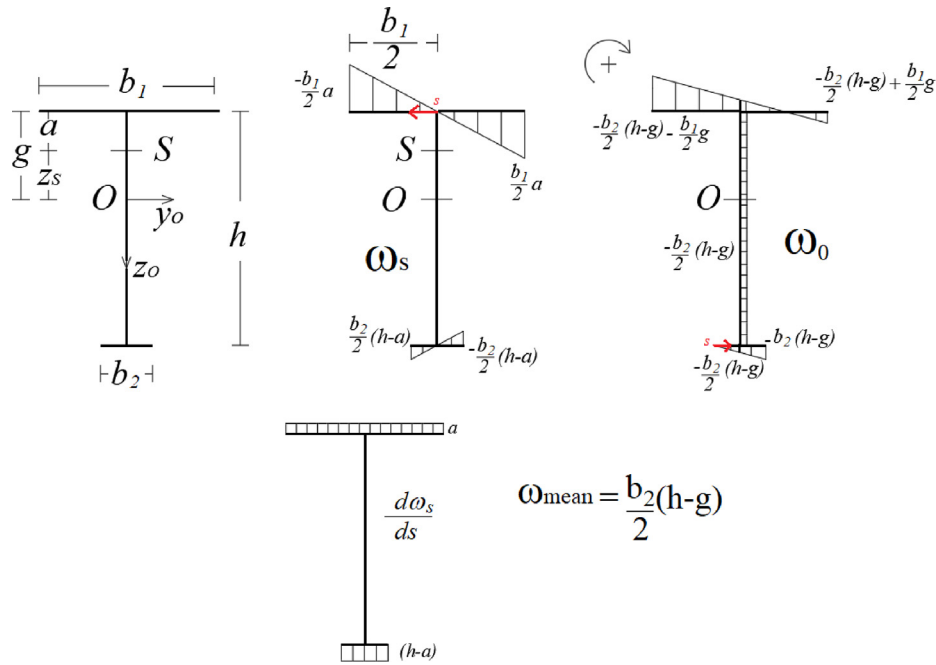
Fig. 7. *Distribution of ω_0, ω_s and $d\omega_s/ds$ for a monosymmetric H-shaped section.*
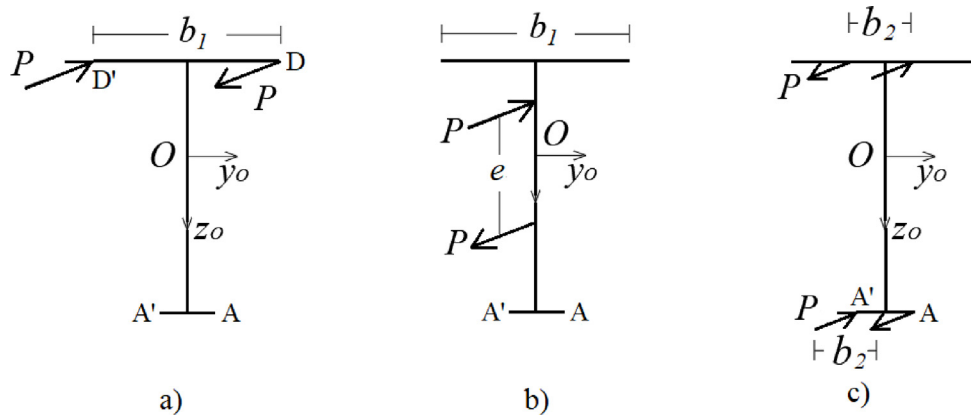

Fig. 8. Different cases of longitudinal forces on a *T* section.

(2) in accordance with Eq. (8), since y_s is nil (i.e. $M_y y_s = 0$) and $z_s = (g\text{-}a)$:

$$B = \left[-P \left(-\frac{b_2}{2}(h-g) - \frac{b_1}{2}g \right) + P(-\frac{b_2}{2}(h-g) + \frac{b_1}{2}g) \right] - \left[Pb_1(g-a) \right] - P \left[\frac{b_2}{2}(h-g) - \frac{b_2}{2}(h-g) \right] = Pb_1 a \tag{13b}$$

(3) in accordance with Eq. (11), by considering that in the top flange the derivate of the sectorial area with respect to the abscissa is constant and equal to a:

$$B = M \left(\frac{\Delta\omega_s}{\Delta s} \right)_k = Pb_1 a \tag{13c}$$

Other two cases of interest for practical design purposes are presented in parts (b) and (c) of Fig. 8. In particular:

• a couple of forces P lying on the web plane, i.e. where the sectorial area is always nil (Fig. 8b), does not generate bimoment;
• a system of self-balanced forces P generating two opposite moments in the plane of the flanges (Fig. 8c) leads to $B = Pb_2 h$.

3. The transformation matrix alternatives

In this paper, for the sake of simplicity, only first-order elastic analysis is considered by using the 7DOFs *beam* element. Attention is herein mainly focussed on the sole assemblage phase to form the global stiffness matrix obtained from the local one associated with each FE *beam*, by using the transformation matrix.

As well known, in the first-order elastic analysis, the effect of the deformed shape of members is neglected and the relationship between global generalised displacement {u} and generalised internal forces {F} depends on the sole global elastic stiffness matrix $[K]^{E,g}$:

$$\{F\} = [K]^{E,g}\{u\} \tag{14}$$

Using j and p to identify the nodes of the *beam* element, the linear algebraic system can be rewritten as:

$$\begin{bmatrix} \{F\}_j \\ \{F\}_p \end{bmatrix} = \begin{bmatrix} [K]_{jj}^{E,g} & [K]_{pj}^{E,g} \\ [K]_{jp}^{E,g} & [K]_{pp}^{E,g} \end{bmatrix} \begin{bmatrix} \{u\}_j \\ \{u\}_p \end{bmatrix} \tag{15}$$

where $[K]_{jj}^{E,g}$, $[K]_{pp}^{E,g}$, $[K]_{pj}^{E,g}$ and $[K]_{jp}^{E,g}$ are the 7×7 sub-matrices; $\{F\}_j$, $\{F\}_p$ and $\{u\}_j$, $\{u\}_p$ are the generalised forces and displacements referred to the node j or p, defined as:

$$\{F\}_{j/p} = \begin{Bmatrix} N \\ F_y \\ F_z \\ M_x \\ M_y \\ M_z \\ B \end{Bmatrix} \qquad \{u\}_{j/p} = \begin{Bmatrix} u \\ v \\ \delta \\ \varphi_x \\ \varphi_y \\ \varphi_z \\ \theta \end{Bmatrix} \tag{16a, b}$$

Therefore, for each *beam* element, the algebraic linear system must be expressed in the global reference system by means the use of the transformation matrix [T], following the rules:

$$[K]^{E,g} = [T][K]^{E,l}[T]^T \tag{17a}$$

$$\{F\} = [T]^T \{F\}^l \tag{17b}$$

$$\{u\} = [T]\{u\}^l \tag{17c}$$

where the vectors with superscript l are intended in the local reference system.

With reference to the *beam* element of length L, by considering its cross-section properties in terms of area (A_g), second moments of area along principal axes (I_z and I_y), de Saint Venant's torsional and warping constants (I_t and I_w, respectively) and by assuming E and G for Young and Tangential material modulus, respectively, the elastic stiffness matrix $[K]^{E,l}$ is defined as:

$$[K]^{E,l} = \begin{bmatrix}
a & . & . & . & . & . & . & -a & . & . & . & . & . & . \\
. & b1 & . & . & . & c1 & . & . & -b1 & . & . & . & c1 & . \\
. & . & b2 & . & -c2 & . & . & . & . & -b2 & . & -c2 & . & . \\
. & . & . & d & . & . & -e & . & . & . & -d & . & . & -e \\
. & . & -c2 & . & f2 & . & . & . & . & c2 & . & g2 & . & . \\
. & c1 & . & . & . & f1 & . & . & -c1 & . & . & . & g1 & . \\
. & . & . & -e & . & . & h & . & . & . & e & . & . & i \\
-a & . & . & . & . & . & . & a & . & . & . & . & . & . \\
. & -b1 & . & . & . & -c1 & . & . & b1 & . & . & . & -c1 & . \\
. & . & -b2 & . & c2 & . & . & . & . & b2 & . & c2 & . & . \\
. & . & . & -d & . & . & e & . & . & . & d & . & . & e \\
. & . & -c2 & . & g2 & . & . & . & . & c2 & . & f2 & . & . \\
. & c1 & . & . & . & g1 & . & . & -c1 & . & . & . & f1 & . \\
. & . & . & -e & . & . & i & . & . & . & e & . & . & h
\end{bmatrix} \tag{18}$$

$$a = \frac{EA_g}{L}; b1 = \frac{12EI_z}{L^3}; b2 = \frac{12EI_y}{L^3}; c1 = \frac{6EI_z}{L^2}; c2 = \frac{6EI_y}{L^2}; d = \frac{GI_t}{L} + \left\{\frac{12EI_w}{L^3} + \frac{GI_t}{5L}\right\}; e = \left\{\frac{6EI_w}{L^2} + \frac{GI_t}{10L}\right\}$$

$$f1 = \frac{4EI_z}{L}; f2 = \frac{4EI_y}{L}; g1 = \frac{2EI_z}{L}; g2 = \frac{2EI_y}{L}; h = \left\{\frac{4EI_w}{L} + \frac{2GI_tL}{15}\right\}; i = \left\{\frac{2EI_w}{L} - \frac{GI_tL}{30}\right\} \tag{19}$$

The cross-section of the FE *beam* is referred to a global reference system axis (X,Y,Z), having its origin in point $\overline{O}$, as showed in Fig. 9. The centroid of the cross-section, O, that is the origin of the local (beam) reference system, is eccentric (y_o, z_o) with respect to the global reference system. The shear centre is identified by point S (h_s, b_s). The eccentricity between the centroid and the shear centre is identified by y_s and z_s. Term
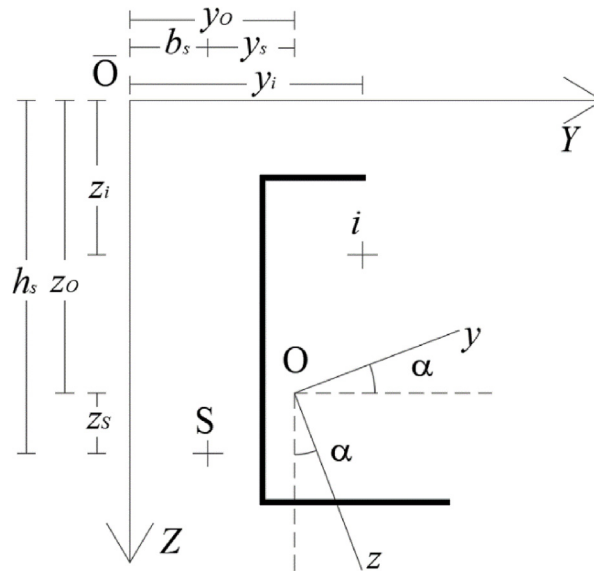
Fig. 9. Arbitrary position of the cross-section beam element in global system (X, Y, Z).

α expresses the angle between the principal axes of the cross-section in the local reference system and the axes of the global reference system. The generic loaded point is, in the following, identified with y_i and z_i.

As previously introduced (Fig. 1b), the nodal parameters are defined with respect to the shear centre or to the centroid in the local reference system. For the assembly phase it is necessary, to referred them to the global reference system. It is worth noting that, for the generic node of a *beam* element with non-symmetric cross-section, after the transformation from the local to the global reference system, shear forces and bending moments depend on the α angle, as it follows:

$$N_{\overline{O}} = N_O \tag{20a}$$

$$F_{y\overline{O}} = F_y \cos\alpha + F_z \sin\alpha \tag{20b}$$

$$F_{z\overline{O}} = -F_y \sin\alpha + F_z \cos\alpha \tag{20c}$$

$$M_{y\overline{O}} = M_y \cos\alpha + M_z \sin\alpha - N_O z_i \tag{20d}$$

$$M_{z\overline{O}} = -M_y \sin\alpha + M_z \cos\alpha + N_O y_i \tag{20e}$$

The torsional moment in the global reference system has to include also the contribution of the shear forces eccentricities with respect to the cross-section shear centre:

$$M_{x\overline{O}} = M_x + F_y[-(h_s - z_i)\cos\alpha + (y_i - b_s)\sin\alpha] - F_z[(y_i - b_s)\cos\alpha + (h_s - z_i)\sin\alpha] \tag{20f}$$

As to the bimoment, it is evaluated in commercial 7DOFs beam FEAPs, by means of two different alternatives, in the following identified as alternative 1 (Alt. 1) and alternative 2 (Alt. 2).

In Alt. 1, the bimoment in the global reference system, is expressed in term of the bimoment referred to the shear centre plus the bimoment generated from the axial force and bending moments contributions, in accordance with the first and second Vlasov's theorems. As a consequence, by considering Eq. (8), it results that:

$$B_{\overline{O}} = B - N_O W - M_y \left[(y_i - b_s)\cos\alpha + (h_s - z_i)\sin\alpha \right] + M_z[(h_s - z_i)\cos\alpha + (y_i - b_s)\sin\alpha] \tag{21a}$$

where term W is defined as: $W = \omega_0\left(y_i, z_i\right) - \omega_{mean}$.

In Alt. 2, the bimoment in the global reference system is assumed to be coincident with the one acting on the shear centre of the cross-section, i.e. expressed in the local reference system:

$$B_{\overline{O}} = B \tag{21b}$$

It is hence possible to derive the transformation matrix [T], which depends by the considered alternatives, owing to the different strategies adopted to transform the bimoment.

- The Alt.1 it considers the coupling between bending moments, axial force and bimoment. The transformation matrix is:

$$[T]^{Alt.1} = \begin{bmatrix} 1 & 0 & 0 & 0 & -z_i & y_i & -W \\ 0 & \cos\alpha & \sin\alpha & -(h_s - z_i)\cos\alpha + (y_i - b_s)\sin\alpha & 0 & 0 & 0 \\ 0 & -\sin\alpha & \cos\alpha & -(y_i - b_s)\cos\alpha - (h_s - z_i)\sin\alpha & 0 & 0 & 0 \\ 0 & 0 & 0 & 1 & 0 & 0 & 0 \\ 0 & 0 & 0 & 0 & \cos\alpha & \sin\alpha & -(y_i - b_s)\cos\alpha - (h_s - z_i)\sin\alpha \\ 0 & 0 & 0 & 0 & -\sin\alpha & \cos\alpha & (h_s - z_i)\cos\alpha + (y_i - b_s)\sin\alpha \\ 0 & 0 & 0 & 0 & 0 & 0 & 1 \end{bmatrix}$$

(22a)

- The Alt.2 neglects the coupling between bending moments and bimoment. The transformation matrix is:

$$[T]^{Alt.2} = \begin{bmatrix} 1 & 0 & 0 & 0 & -z_i & y_i & 0 \\ 0 & \cos\alpha & \sin\alpha & -(h_s - z_i)\cos\alpha + (y_i - b_s)\sin\alpha & 0 & 0 & 0 \\ 0 & -\sin\alpha & \cos\alpha & -(y_i - b_s)\cos\alpha - (h_s - z_i)\sin\alpha & 0 & 0 & 0 \\ 0 & 0 & 0 & 1 & 0 & 0 & 0 \\ 0 & 0 & 0 & 0 & \cos\alpha & \sin\alpha & 0 \\ 0 & 0 & 0 & 0 & -\sin\alpha & \cos\alpha & 0 \\ 0 & 0 & 0 & 0 & 0 & 0 & 1 \end{bmatrix}$$

(22b)

As highlighted in the following section, the choice of the transformation matrix, i.e. the use of matrix (22a)) or Eq. (22b), could lead to remarkably different results in term of structural response. More details related to practical applications of these matrices can be found in Appendix, where one of the cases discussed in the next session is reproduced.

4. Numerical applications on mono-symmetric cross-section members

As already discussed, the transformation matrices associated with alternative 1 (Eq. (22a) or 2 (Eq. (22b) allow for accounting the coupling between flexural moments and bimoment in two different ways to pass from the local to the global reference system. To appraise the differences associated with their use, reference has been made to practical cases related to a cantilever beam fully fixed at one end and loaded at the free one. Four different loading conditions have been considered, namely:

- shear force parallel to the web;
- bending moment along a plane parallel to the web;
- bending moment along a plane parallel to the flanges;
- eccentric axial force.

This basic structure was selected so as to allow for a direct reproduction of the results both theoretically, via the mixed torsion theory, and numerically, via refined FE *shell* models. The two transformation matrices have been implemented in a finite element analysis open-source programme developed by the Authors for academic research and already used in previous papers [26]. Several FE formulations have been added over the years and the last one is represented by the 7DOFs *beam* element developed in accordance with [4]. As to the FE models via *shell* elements, the commercial analysis software ABAQUS [16] has been used by accurately meshing the member with S4R elastic *shell* elements. Furthermore, in order to reproduce the cantilever boundary conditions, a mask at the fixed end was applied via the use of wire elements connected to the section centroid. Moreover, at the free end the load (i.e. a force or bending moment) was applied to the cross-section centroid, which was connected only to the web, to allow for free warping.

As to the theory, an external torsional moment $M_x(x)$ can be split into the Saint-Venant, $M_t(x)$, and the warping torsion, $M_\omega(x)$, contributions. Given that, in the proposed examples there is not applied a distributed torsional moment, the torsion is expressed as:

$$M_x(x) = M_\omega(x) + M_t(x) = GI_t \frac{d\varphi_x}{dx} - EI_w \frac{d^3\varphi_x}{dx^3}$$

(23)

where E and G are the Young and the shear modulus, respectively.

The general solution of Eq. (23) is:

$$\varphi_x(x) = C1 + C2\sinh(\lambda_T x) + C3\cosh(\lambda_T x) + \varphi_{ip}$$

(24)

where *C1, C2* and *C3* are integration constants depending on the boundary conditions; φ_{ip} is the particular solution associated with the assigned load conditions and λ_T is the relative torsional slenderness defined as:

$$\lambda_T = \sqrt{\frac{GI_t}{EI_w}}$$

(25)

The two boundary conditions that are valid for all the cases herein considered are:

- no torsion at the fixed end, i.e. $\varphi_x(0) = 0$
- no warping at the fixed end, i.e. $\varphi'_x(0) = 0$

Table 1
Geometrical data of the considered cross-sections.

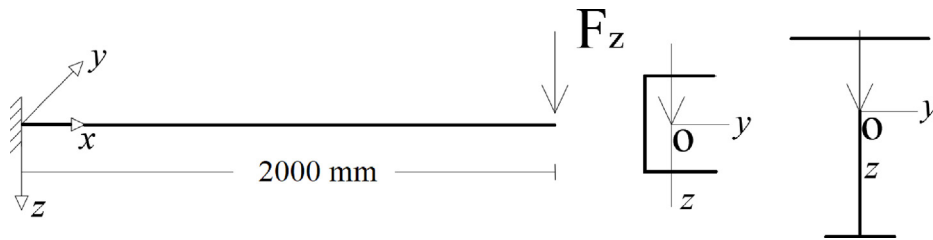|	EFC	UFI
A_g [mm^2]	$4.92\cdot10^2$	$26.00\cdot10^2$
t [mm]	2.0	5.0
I_y [mm^4]	$86.76\cdot10^4$	$34.79\cdot10^4$
I_z [mm^4]	$29.65\cdot10^4$	$15.85\cdot10^4$
I_t [mm^4]	656	$22.36\cdot10^3$
I_w [mm^9]	$50.0\cdot10^7$	$14.1\cdot10^9$
y_s [mm]	52.57	0.0
z_s [mm]	0.0	94.70
$|\omega_{s,max}|$ [mm^2]	$21.41\cdot10^2$	10^4
λ_T	$7.10\cdot10^{-4}$	$7.72\cdot10^{-4}$

Fig. 10. Cantilever beam with the shear force applied in the cross-section centroid, point O.

The third boundary condition depends on the load case under consideration, as detailed in the following.

By considering the torsional effects, the maximum lateral and vertical displacements at the free end ($\delta(L)$ and $v(L)$, respectively) are obtained by combining the classic flexural contribution with the torsional one:

$$\delta(L) = \delta_F(L) + \delta_\omega(L) \tag{26a}$$

$$v(L) = v_F(L) + v_\omega(L) \tag{26b}$$

For each load case, two different mono-symmetric cross-sections have been considered: an equal flange plain channel (EFC) and an unequal flange I-shaped profile (UFI). Table 1 contains the main geometrical data of these cross-sections and presents the values of the main cross-sectional properties together with the thickness (t) and the maximum value of the sectorial area ($\omega_{s,max}$). Furthermore, the eccentricities between the cross-section centroid and the shear centre together with the torsional slenderness (λ_T), are reported too.

The geometrical data presented in Table 1 have been evaluated directly by using the simplified procedure reported in Appendix C of the EC3-1-3 [27]. In particular, each cross-section has been meshed via suitable sets of points and segments. It is worth noting that the degree of accuracy in predicting geometrical cross-section data is more than acceptable, as discussed also by Ziemian et al. [28], which generally agree with the same geometrical data obtained from closed form theoretical expressions. As to the material properties, it has been assumed $E = 210,000$ MPa and $v = 0.3$ and the constitutive law has been considered perfectly elastic, due to the scope of this research.

4.1. Shear force parallel to the web

The beam is loaded by a vertical force equal to $F_z = 1.0$ kN, parallel to the web and applied on the centroid of the free end cross-section of the cantilever beam (Fig. 10). In EFC member, there is an eccentricity between the shear centre and the loaded point. Consequently, a torsional moment acts at the free end, equal to $M_x(L) = F_z \cdot y_s$. For the UFI cross section member, torsion is nil, being the shear centre on the load application line.
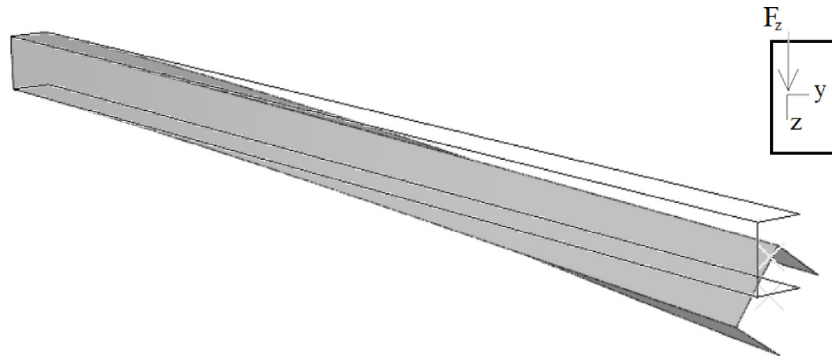
Fig. 11. Deformed shape of EFC with FE shell elements.

Table 2
Key results of the first-order elastic analysis with a shear force applied.

		EFC	UFI
FE *beam* Alt. 1	B [kNm²] (x=0)	-62810	0.0
	M_x [kNm] (x=L)	52.57	0.0
	φ_x [rad] (x=L)	-0.742	0.0
	δ [mm] (x=L)	53.61	0.359
FE *beam* Alt. 2	B [kNm²] (x=0)	-62811	0.0
	M_x [kNm] (x=L)	52.57	0.0
	φ_x [rad] (x=L)	-0.742	0.0
	δ [mm] (x=L)	53.60	0.359
theory	B [kNm²] (x=L)	-62758	0.0
	φ_x [rad] (x=L)	-0.741	0.0
	δ [mm] (x=L)	53.52	0.359
FE *shell*	φ_x [rad] (x=L)	-0.739	0.0
	δ [mm] (x=L)	52.62	0.357

For the EFC member, the particular solution is:

$$\varphi_{ip} = \frac{F_z \cdot y_s}{G \cdot I_t} x \tag{27}$$

The third necessary condition to evaluate the set of the general solution constants (C1, C2 and C3) is represented by a bimoment, $B(x) = EI_w \varphi_x''(x)$, nil at the free end, reflecting in the condition: $\varphi_x''(L) = 0$.

The expression of the torsional rotation is thus:

$$\varphi_x(x) = \frac{F_z y_s}{\lambda_T G I_t} \left[\lambda_T x + \frac{\sinh(\lambda_T (L - x))}{\cosh(\lambda_T L)} - \tanh(\lambda_T L) \right] \tag{28}$$

The bimoment distribution along the cantilever is:

$$B(x) = -\frac{F_z y_s}{\lambda_T} \cdot \frac{\sinh(\lambda_T (L - x))}{\cosh(\lambda_T L)} \tag{29a}$$

Therefore, at the fixed end cross-section, i.e. with $x = 0$, the bimoment is maximum and equal to:

$$B(0) = -\frac{F_z y_s}{\lambda_T} \cdot \tanh(\lambda_T L) \tag{29b}$$

Finally, at the free end, the maximum vertical displacement (δ) referred to cross-section centroid is expressed as:

$$\delta(L) = \delta_F(L) + \delta_\omega(L) = \frac{F_z L^3}{3EI_y} + y_s \varphi_x(L) = \frac{F_z L^3}{3EI_y} + y_s \frac{F_z y_s}{\lambda_T G I_t} \left[\lambda_T L - \tanh(\lambda_T L) \right] \tag{30}$$

Therefore, with the load on the centroid, EFC response is governed by the torsional rotation. On the contrary, the UFI profile is in simple bending. The deformed shape of ECF obtained from the FE *shell* model is reported in Fig. 11. The relevance of the torsion of the beam can be noted at its free end.

Main results related to the two alternative FE approaches together with the ones associated with the theoretical solution and with the FE *shell* models are reported in Table 2. In particular, the bimoment, $B(0)$, is reported at the fixed end, whereas for the free end reference is made to the values of the total torsional moment, $M_x(L)$, the torsional rotation, φ_x (L), and the vertical displacement, δ(L).

It can be noted that both results associated with the FE *beam* alternatives are equivalent and differences with the theory are never greater than 0.1%. Furthermore, the more than satisfactory correspondence between the data in the table and the ones obtained via FE *shell* models confirm the accuracy of the mesh as well as of the strategies adopted to model the restraints and the load application. Focussing attention on the EFC cantilever, the non-negligible influence of the bimoment on the overall behaviour can be appreciated also by considering the normal stresses
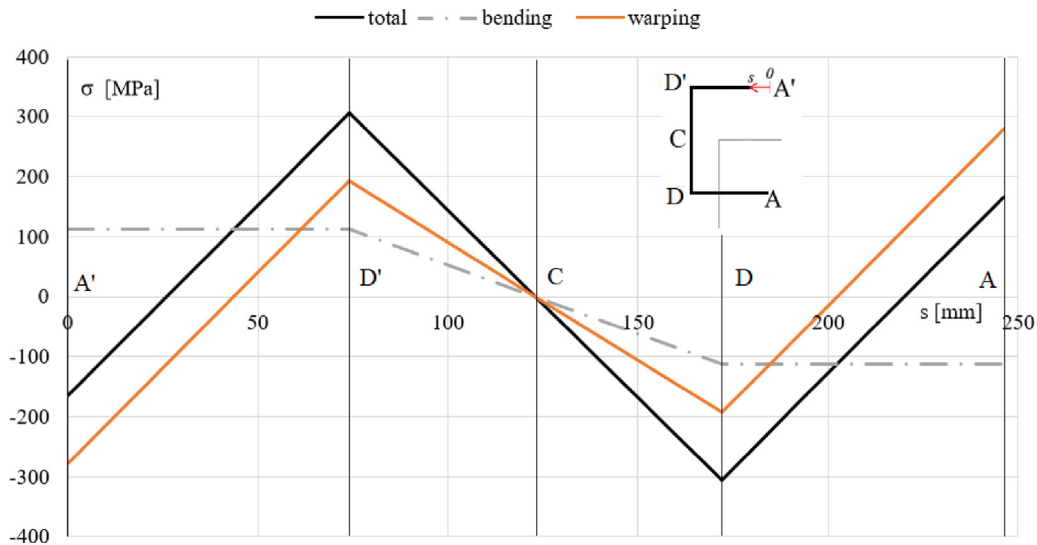
Fig. 12. Bending (σ_F), warping (σ_w) and total stresses ($\sigma = \sigma_F + \sigma_w$) distribution on EF-C cross-section at the fixed end cross section of the cantilever beam (x=L).
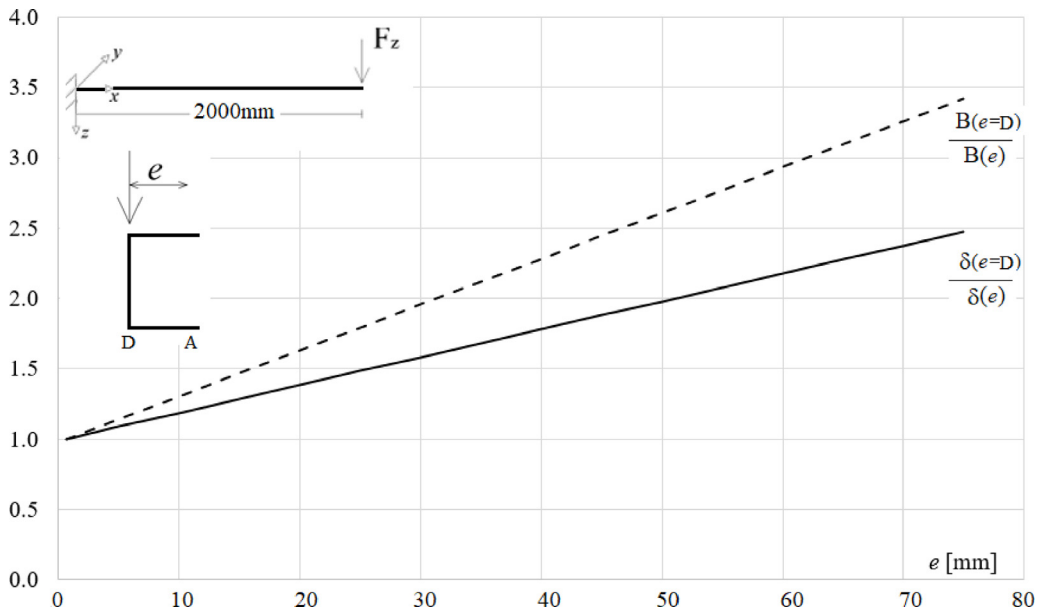

Fig. 13. Warping influence on EFC member by moving the transversal force.

distribution (Eq. (6)), which are displayed in Fig. 12 with reference to the fixed end cross-section (i.e. x=0). In particular, the bending (σ_F) and warping (σ_w) stresses are plotted together with the total one ($\sigma = \sigma_F + \sigma_w$) versus the coordinate s, describing the cross-section midline contour. It is worth noting that in presence of the internal corners D and D' the stress σ_w is about 1.7 times σ_F, confirming the inadequacy of traditional 6 DOFs *beam* formulations in capturing the mono-symmetric cross-section response.

Furthermore, for EFC member Fig. 13 shows the influence of the load application point on the bimoment value at the fixed end. The load application point, expressed by its distance e from the web, was moved along the upper flanges, with e ranging from 0 (load on the web) to 74 mm (load on the flange free end). The results are independent of the transformation matrix (Alt. 1 equal to Alt. 2) and the influence of the warping on the normal stresses and on the displacement increases linearly by moving away from the shear centre.

In the same way, by moving the load application point along the upper flange of the UFI profile, a torsional moment takes place, $M_x(L) = F_z \cdot e$, without influencing the global vertical displacement (δ), which remains a pure flexural displacement due to the cross-section shape. Nevertheless, the lateral displacement (v), evaluated with respect to the centroid, becomes different from zero and increases as the distance of the load from the shear centre increases:

$$v(L) = v_\omega(L) = z_s \varphi_x(L) = z_s \frac{F_z e}{\lambda_T G I_t} \left[\lambda_T L - \tanh\left(\lambda_T L\right) \right] \tag{31}$$

Furthermore, the global deformation obtained from the FE *shell* model for the UFI profile can be appraised from Fig. 14.

Finally, the influence of the beam length L on the results for the EFC member has been investigated. A vertical load was applied on the centroid and the total length was changed from 1 m to 6 m. Main results related to the warping influence are displayed in Fig. 15 where the ratios δ_ω/δ
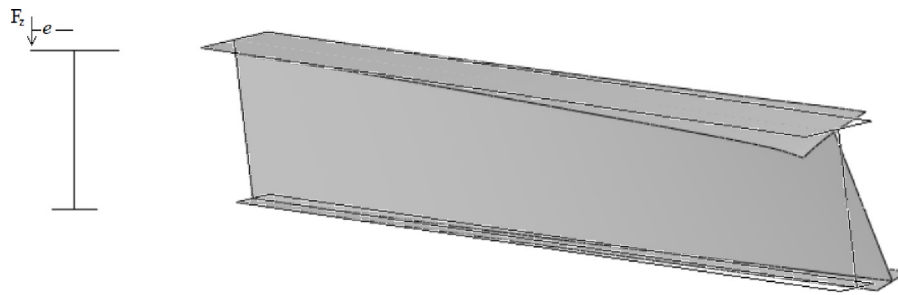
Fig. 14. Deformed shape of UFI with FE shell elements and eccentric vertical load.
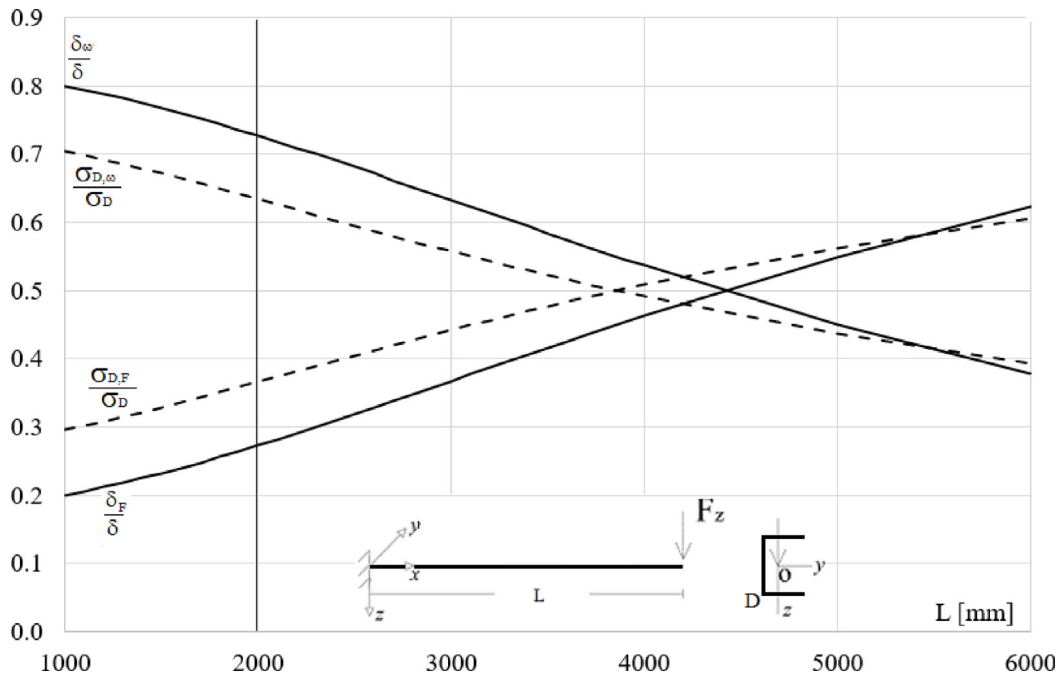

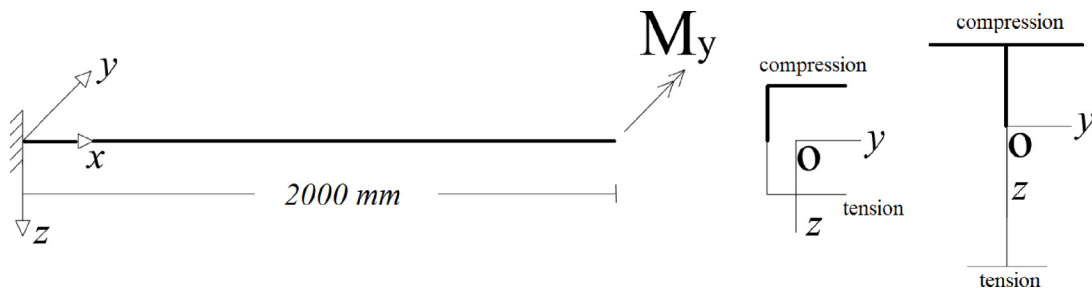**Fig. 15.** Warping influence on EFC member by changing the total length.

Fig. 16. Cantilever beam with the bending moment along the *y*-axis centroid, point O.

and δ_F/δ, i.e. the warping and the flexural contribution over the total displacement are plotted versus L. Furthermore, from the same figure, the stress ratios $\sigma_{D,\omega}/\sigma_D$ and $\sigma_{D,F}/\sigma_D$, evaluated with Eq. (6), related to the point D of the cross-section, can be appraised.

It is worth noting that when increasing L warping influence decreases and the flexural contribution acquires more importance for both the displacements and normal stresses; in any case, it is never negligible for practical design purposes.

4.2. Bending moment along a plane parallel to the web

The cantilever beam's free end is loaded by a bending moment about the strong (*y*) axis, applied on the centroid and equal to $M_y = 1000$ kN mm for both the cross-section types (Fig. 16).

In this case, the external torque is nil and as a consequence, the particular solution is also nil, i.e. $\varphi_{ip} = 0$. The third boundary condition is the bimoment value, given by. Eq. (8). In accordance with Vlasov's second theorem, a bimoment is expected for x=L that is nil for UFI member, being

Table 3
First-order elastic analysis with a bending moment about the strong axis.

		EFC	UFI
FE *beam* Alt. 1	B [kNmm²] (x=0)	-24005	0.00
	B [kNmm²] (x=L)	-52570	0.00
	φ_x [rad] (x=L)	-0.539	0.00
	δ [mm] (x=L)	39.33	0.269
FE *beam* Alt. 2	B [kNmm²] (x=0)	**0.00**	0.00
	B [kNmm²] (x=L)	**0.00**	0.00
	φ_x [rad] (x=L)	**0.00**	0.00
	δ [mm] (x=L)	**10.98**	0.269
theory	B [kNmm²] (x=0)	-24002	0.00
	B [kNmm²] (x=L)	-52570	0.00
	φ_x [rad] (x=L)	0.539	0.00
	δ [mm] (x=L)	39.29	0.269
FE *shell*	φ_x [rad] (x=L)	0.503	0.00
	δ [mm] (x=L)	36.03	0.268

$y_s = 0$, and for the EFC one is equal to: $B(L) = M_y y_s$. The final expression of the rotation is equal to:

$$\varphi_x(x) = \frac{M_y y_s}{\lambda_T^2 \cosh(\lambda_T L)} \left(1 - \cosh(\lambda_T x) \right) \tag{32}$$

The bimoment distribution along the member is described by the equation:

$$B(x) = M_y y_s \frac{\cosh(\lambda_T x)}{\cosh(\lambda_T L)} \tag{33a}$$

At the restrained end, the bimoment assumes its minimum value, that is:

$$B(0) = M_y y_s \frac{1}{\cosh\left(\lambda_T L\right)} \tag{33b}$$

The maximum vertical displacement at the free end is therefore equal to:

$$\delta(L) = \delta_F(L) + \delta_\omega(L) = \frac{M_y L^2}{2 E I_y} + y_s \frac{M_y y_s}{\lambda_T^2 \cosh(\lambda_T L)} \left(1 - \cosh(\lambda_T L) \right) \tag{34}$$

Main results related to the two alternative approaches for the FE *beam* formulation with the ones obtained via the theoretical solution and via the FE *shell* models are reported in Table 3.

As to the UFI members, no differences between the results associated with Alt. 1 and Alt. 2 can be observed, which, as in the previous examples, practically coincide with the theoretical ones as well as with the ones associated with the FE *shell* model. This is due to the fact that, in accordance with Eq. (8) the shear centre eccentricity is nil for the considered moment.

Furthermore, if the ECF member is considered, Alt.1 is the sole able to correctly capture the coupling between the bending moments and the bimoment. In fact, the approximations of the rotation and vertical displacement are less than 5% and 3%, respectively, and the bimoment practically coincides with both theoretical and FE *shell* results. By using Alt.2, the effects associated with the coupling between torsion and bending cannot be captured: bimoment is in fact nil and the vertical displacement is 3.5 times less than the effective one. Of course, also the stress distribution remarkably depends on the considered alternative, as it appears from Fig. 17 where the total normal stresses are plotted versus the co-ordinate *s* describing the perimeter of the cross-section. Differences in the stresses are up to 4 times different and in points D and D' the effective stress is more than two times greater than the one associated with Alt. 2, that considers, for this case, only flexural stresses as the traditional 6DOFs beam FE formulations.

Finally, the influence of the beam length L has been investigated for Alt.1. Key results are proposed in Fig. 18, where the ratios δ_ω/δ and $\sigma_{D,\omega}/\sigma_D$ are plotted versus L, ranging from 1 m to 6 m. It should be noted that, by increasing the length of the beam, the warping influence decreases and the flexural contribution becomes more important for both the displacements and normal stresses. However, also for the maximum length (L=6 m), the influence of the warping is up to 8% on the stresses and almost 40% on the vertical displacement.

4.3. Bending moment along a plane parallel to the flanges

The third case is related to a cantilever beam subjected to a bending moment applied about the weak (z) axis to the centroid of the free end cross-section, equal to $M_z = 1000$ kN mm (Fig. 19). As to the FE *beam* formulation, bending moment is applied directly to the correspondent rotational degree of freedom. Key results are proposed in Table 4.

The theoretical expressions are exactly the ones already reported in Section 4.2. The only difference is that, in this case, the vertical displacement, δ, is always nil because of the bending along the weak axis. As a consequence, the transformation matrix correctly acts only on the transversal displacement, *v*.

The response of the EFC member is not influenced by the choice of the transformation matrix. Furthermore, in case of UFI beam, Alt.2 is not able to capture the correct member response, ignoring the presence of the rotation as well as of the bimoment, with the consequence that the lateral displacement is approximately 1.5 times lower than the effective one.
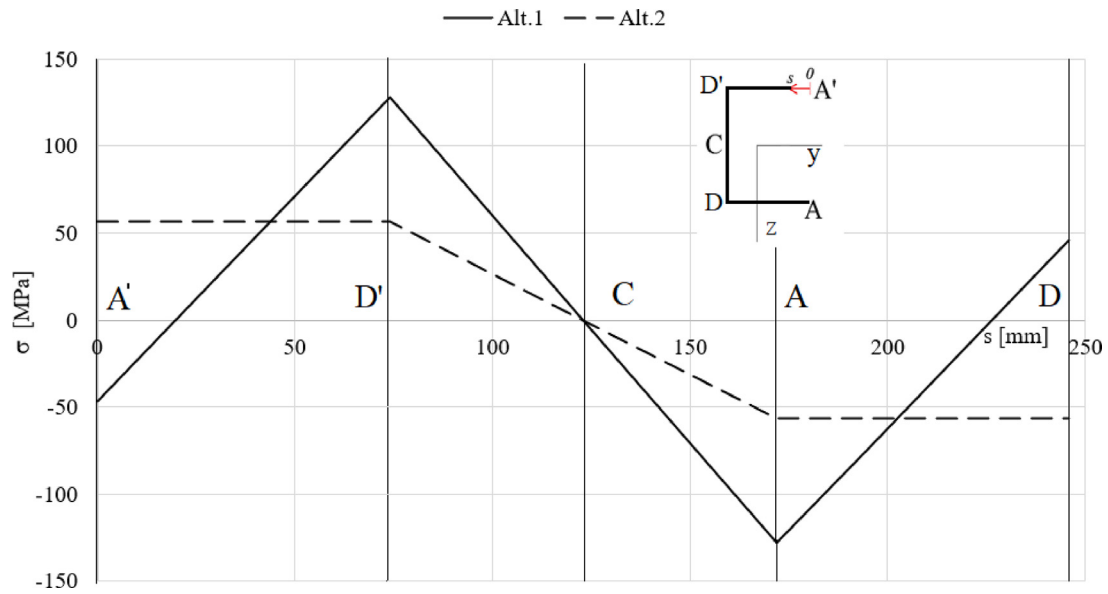
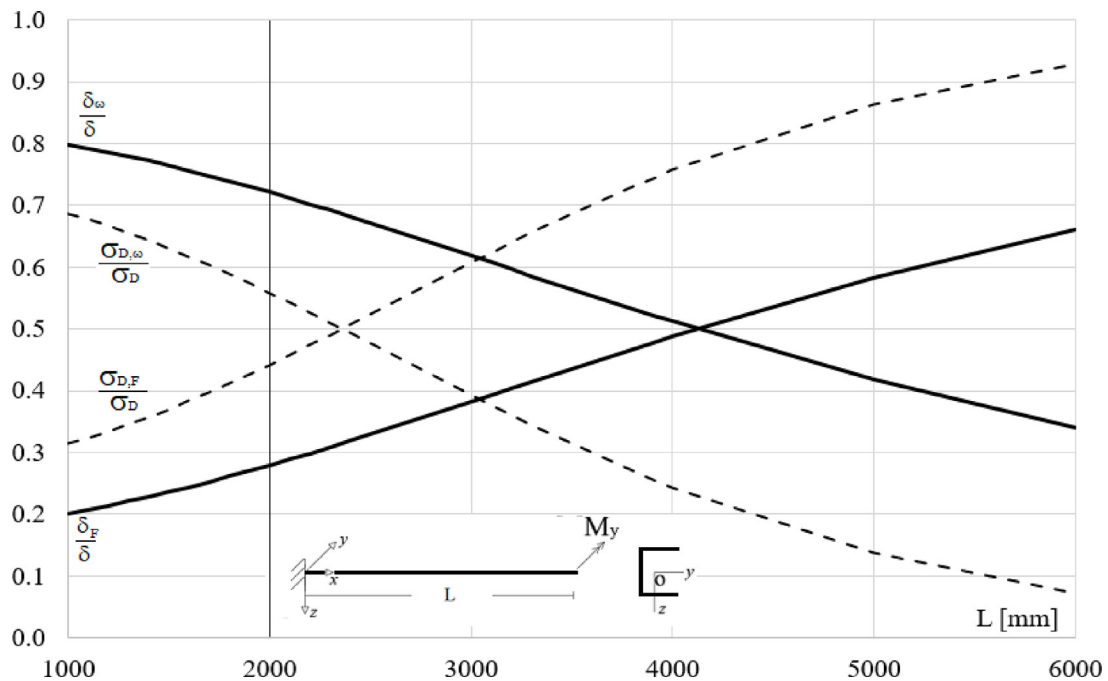Fig. 17. Total stresses with the two alternatives, bending moment on cantilever beam.

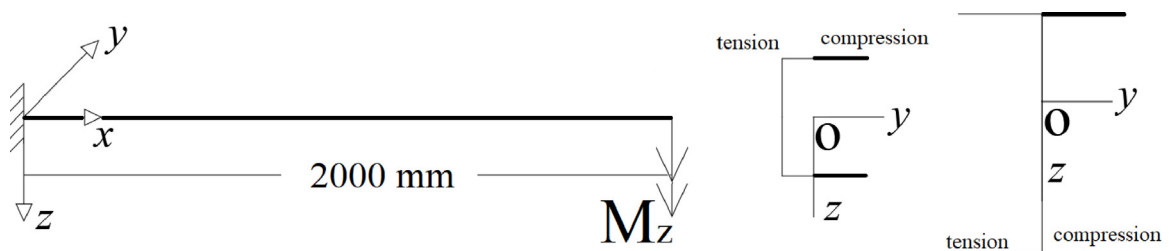Fig. 18. Warping influence on ECF member by changing the total length.

Fig. 19. The case of the cantilever beam with the bending moment along the z-axis.

To understand the influence of the warping effects by changing the total length (L) of the UFI beam, Fig. 20 can be considered, where the total lateral displacement due to the warping contribution, v_ω, over the total displacement, v, and the ratio between the warping stress, $\sigma_{D,\omega}$, and

Table 4
First-order elastic analysis with a bending moment about the weak axis.

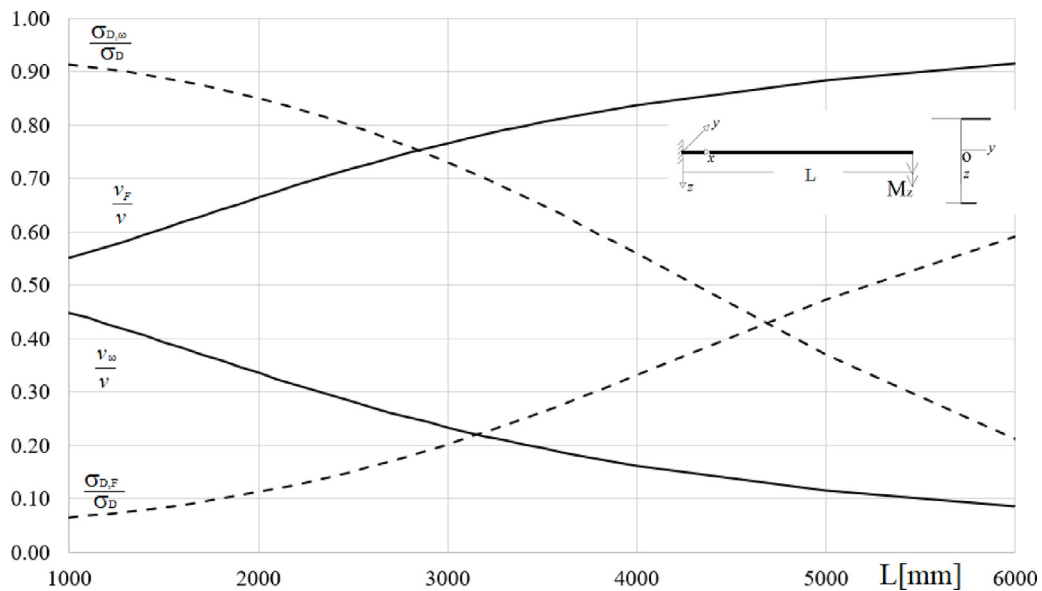|		EFC	UFI
FE *beam* Alt. 1	B [kNmm²] (x=0)	0.00	38700
	B [kNmm²] (x=L)	0.00	95240
	φ_x [rad] (x=L)	0.00	0.0321
	v [mm] (x=L)	32.12	8.92
FE *beam* Alt. 2	B [kNmm²] (x=0)	0.00	**0.00**
	B [kNmm²] (x=L)	0.00	**0.00**
	φ_x [rad] (x=L)	0.00	**0.00**
	v [mm] (x=L)	32.11	**6.02**
theory	B [Nmm²] (x=0)	0.00	38366
	B [Nmm²] (x=L)	0.00	95240
	φ_x [rad] (x=L)	0.00	0.0319
	v [mm] (x=L)	32.12	9.00
FE *shell*	φ_x [rad] (x=L)	0.00	0.0356
	v [mm] (x=L)	32.12	9.46

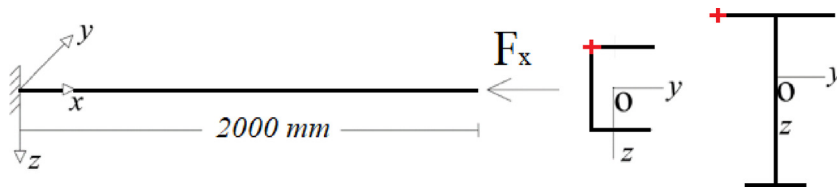**Fig. 20.** Warping influence on UFI member by changing the total length.

Fig. 21. Cantilever beam with eccentric axial force.

the total stress, σ_D, at point D, are plotted versus L. It should be noted that, also in this case, by increasing the length of the beam, the warping influence decreases and the flexural contribution becomes more important for both the displacements and normal stresses, but it is never negligible for practical design purposes.

4.4. Eccentric axial force

The last case is related to a cantilever beam subjected to an eccentric axial force, $F_x=-1.0$ kN, applied at the top flange of the considered cross-sections (Fig. 21).

As discussed in Section 2, both bimoment and torsional rotation take place, depending on the value of the sectorial area of the specific point where the eccentric axial force is applied. Consequently, the total vertical displacement (δ) is obtained by combining the contribution of the flexure with the one due to the torsion. In Table 5, key results of the different analyses can be appraised. As in the previous cases, Alt. 2 is inadequate to capture the effective member behaviour. Conversely, Alt. 1 allows for a correct appraisal of the cantilever response, as demonstrated by the

Table 5
Key results of the first-order elastic analysis with an eccentric axial force applied.

|		EFC	UFI
FE *beam* Alt. 1	B [kNmm²] (x=0)	670	903.2
	B [kNmm²] (x=L)	1485.5	2500
	φ_x [rad] (x=L)	0.0152	0.00084
	v [mm] (x=L)	-0.71	0.37
	δ [mm] (x=L)	1.33	0.035
FE *beam* Alt. 2	B [kNmm²] (x=0)	**0.00**	**0.00**
	B [kNmm²] (x=L)	**0.00**	**0.00**
	φ_x [rad] (x=L)	**0.00**	**0.00**
	v [mm] (x=L)	**-0.72**	**0.45**
	δ [mm] (x=L)	**0.54**	**0.035**
theory	B [Nmm²] (x=0)	678.5	1000
	B [Nmm²] (x=L)	1475.5	2500
	φ_x [rad] (x=L)	0.0155	0.00082
	v [mm] (x=L)	-0.71	0.372
	δ [mm] (x=L)	1.34	0.034
FE *shell*	φ_x [rad] (x=L)	0.0156	0.0074
	v [mm] (x=L)	-0.71	0.38
	δ [mm] (x=L)	1.36	0.034

Uprights cross-section
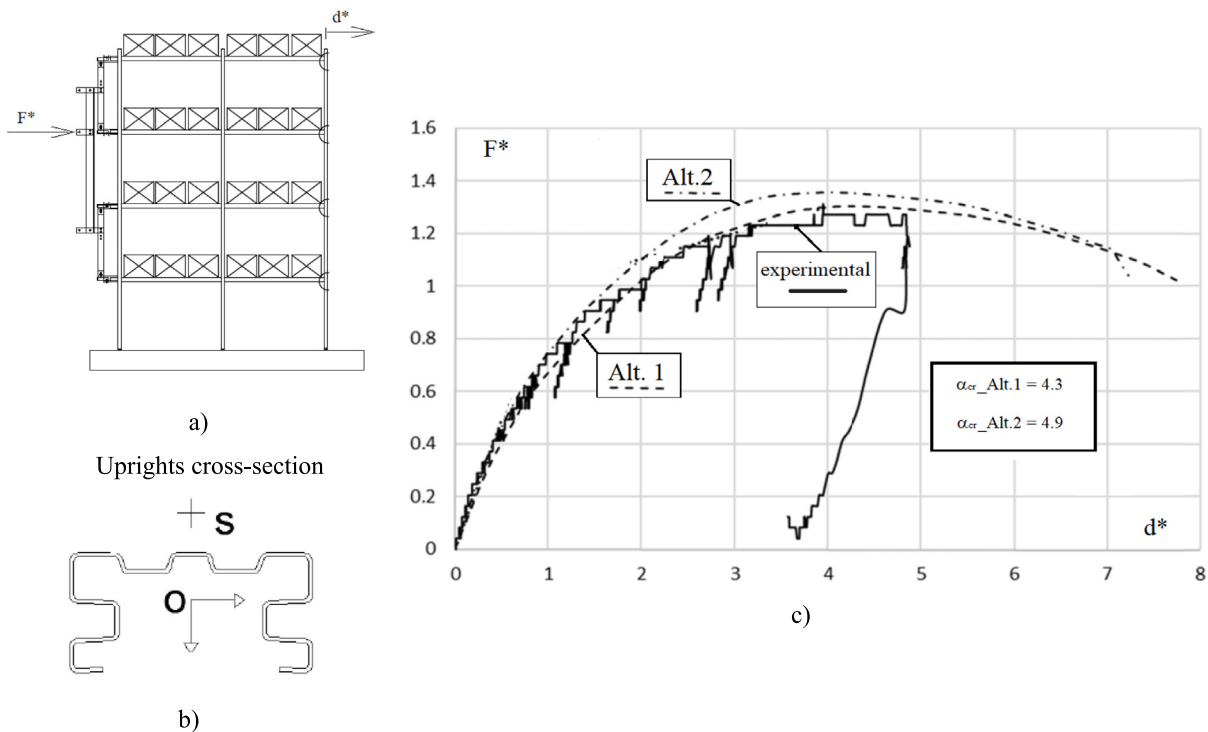
Fig. 22. Test layout scheme of a spatial rack frame (a) and non-dimensional experimental and numerical curves (b) [26].

theoretical as well as FE *shell* simulation results. The only exception is represented by the *B(0)* for the UFI member, as the difference against the theoretical value is approximately 10%, which is however acceptable for practical design purposes.

In Appendix, the EFC case has been developed by using the FE matrices and considering a single finite element beam, in order to allow for a direct appraisal of the differences associated with the transformation matrices.

5. Concluding remarks

This paper is focussed on the 7DOFs FE *beam* modelling of non-bisymmetric cross section members and deals with the influence of the interaction between bending moments and bimoment. Two different transformation matrices, used in few commercial FEAPs, to pass from the local to the global reference system are discussed and applied to basic cases that can be also theoretically reproduced. Research outcomes show that these matrices cannot be considered as alternatives. The application of the mixed torsion theory clearly demonstrates that Alt. 2 is not adequate for practical design purposes, as confirmed also by the results obtained via refined FE *shell* models.

It is worth noting that the considered applications have been focussed on cantilever beams because of the need of proposing examples that could be easily reproduced by readers both theoretically and numerically. The non-negligible influence of the transformation matrix stressed in the paper can also be expected for spatial frames, for which the theoretical approaches cannot be directly applied. In order to allow for a concrete appraisal of these differences, which are expected to influence remarkably the FE output data for design verification checks, the spatial frame depicted in Fig. 22a has been considered. The structure is a steel storage pallet rack with two bays and four load levels experimentally tested in the framework of research project [29]. Bay length and inter-storey height are 4 m and 2 m, respectively. The vertical members (uprights) are lipped channels with rears, characterised by the presence of a cross-section with a sole axis of symmetry (Fig. 22b). The beams have a thin-walled boxed cross-section and both beam-to-column joints and base-plate connections are semi-rigid, as it results from the component tests carried out in accordance with the rack standard provision EN15512 [30]. Overall full-scale frame tests have been carried out by pushing rack in the down-aisle direction by means of a hydraulic jack. Loads have been suitably applied on each storage level in order to simulate an inverse triangular pattern reproducing the deformed modal shape associated with the fundamental period of vibration. Tests were carried out by increasing the value of the applied horizontal forces until collapse was achieved and/or the deformed shape of the rack was in the softening branch and beyond the range of interest for engineering purposes due to the large values of horizontal displacements. For this rack, the numerical responses (Fig. 22c) associated with the transformation matrices have been compared with experimental one (solid line), by considering the non-dimensional relationship between the displacement (d*=d/d_y) and the resulting of the lateral forces (F*=F/F_y) applied during the pushover test. In particular, the total lateral force (F) has been divided by the yielding one (F_y) and the top displacement (d) has been divided by the one corresponding to the yielding force (d_y). The influence of the transformation matrices can be appraised by considering the dashed numerical curves: it can be noted that Alt. 2 leads to overestimate both the stiffness and the frame load carrying capacity. Furthermore, with reference to the presence of the sole gravity load, this influence also reflects in different values of the elastic buckling load multiplier α_{cr}: using Alt. 2 the multiplier is 15% greater than the one associated with Alt. 1. From ref. [26] it can be observed that the results obtained with Alt. 2 are practically coincident with the ones obtained by using a 6DOFs *beam* elements (i.e. no warping effects).

Finally, it can be concluded that the presence of the bimoment can never be neglected in the structural design of steel or concrete thin-walled elements [31]. Nevertheless, also by using 7DOFs, the results could be inaccurate as they strictly depend on the transformation matrix being adopted. To this purpose, the examples discussed in the paper can be used by the software developers as benchmarks.

CRediT authorship contribution statement

Claudio Bernuzzi: Writing – review & editing, Writing – original draft, Supervision, Conceptualization. **Marco Simoncelli:** Writing – review & editing, Writing – original draft, Formal analysis, Conceptualization.

Declaration of competing interest

The authors declare that they have no known competing financial interests or personal relationships that could have appeared to influence the work reported in this paper.

Data availability

Data will be made available on request.

Acknowledgements

Appendix. Finite element application

The application discussed in Sub-Section 4.4 is herein reproduced by using a single 7DOF *beam* finite element, due to the need of allowing for a direct appraisal of the differences associated with the transformation matrices. For the sake of simplicity, the origin of the global reference system coincides with the cross-section centroid and $\alpha = 0$ (that is the angle between the main local axes and the ones of the global reference system, see Fig. 9). The force $F_x = -1000$ N is applied to the point D' which has co-ordinate (−22.26 mm, −49 mm). In the following, the lengths are expressed in millimetres and the forces in newtons (see Fig. A.1).

By considering the sectorial area distribution Fig. 5, the result is:

$$W = \omega_0 \left(y_{D'}, z_{D'} \right) - \omega_{mean} = -b\frac{h}{2} + (b+a)\frac{h}{2} = a\frac{h}{2} = 1090.7 \text{ mm}^2 \qquad (A.1)$$
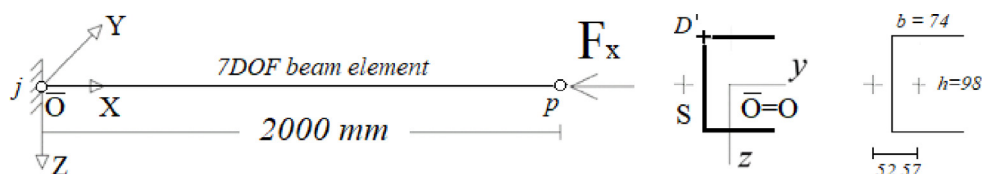
with $a = 22.26$ mm.

Fig. A.1. Cantilever beam with eccentric axial force.

Each node has 7 DOFs and thus the local element stiffness matrix has a range of 14. In accordance with Eq. (18), $[K]^{E,l}$ can be expressed with the associated numerical values as:

$$[K]^{E,l} = \begin{bmatrix} [K]^{E,l}_{jj} & [K]^{E,l}_{pj} \\ [K]^{E,l}_{jp} & [K]^{E,l}_{pp} \end{bmatrix} \tag{A.2a}$$

$$[K]^{E,l}_{pp} = \begin{bmatrix} 5.2 \cdot 10^4 & 0 & 0 & 0 & 0 & 0 & 0 \\ 0 & 93 & 0 & 0 & 0 & -9.3 \cdot 10^4 & 0 \\ 0 & 0 & 273 & 0 & 2.7 \cdot 10^5 & 0 & 0 \\ 0 & 0 & 0 & 1.9 \cdot 10^5 & 0 & 0 & 1.6 \cdot 10^8 \\ 0 & 0 & -2.7 \cdot 10^5 & 0 & 3.6 \cdot 10^8 & 0 & 0 \\ 0 & -9.3 \cdot 10^4 & 0 & 0 & 0 & 1.2 \cdot 10^8 & 0 \\ 0 & 0 & 0 & -1.6 \cdot 10^8 & 0 & 0 & 2.2 \cdot 10^{11} \end{bmatrix} \tag{A.2b}$$

$$[K]^{E,l}_{jp} = \begin{bmatrix} -5.2 \cdot 10^4 & 0 & 0 & 0 & 0 & 0 & 0 \\ 0 & -93 & 0 & 0 & 0 & -9.3 \cdot 10^4 & 0 \\ 0 & 0 & -273 & 0 & 2.7 \cdot 10^5 & 0 & 0 \\ 0 & 0 & 0 & -1.9 \cdot 10^5 & 0 & 0 & 1.6 \cdot 10^8 \\ 0 & 0 & -2.7 \cdot 10^5 & 0 & 1.8 \cdot 10^8 & 0 & 0 \\ 0 & 9.3 \cdot 10^4 & 0 & 0 & 0 & 6.2 \cdot 10^7 & 0 \\ 0 & 0 & 0 & -1.6 \cdot 10^8 & 0 & 0 & 1.1 \cdot 10^{11} \end{bmatrix} \tag{A.2c}$$

The local matrix must be referred to the global system by means the transformation matrix, which for the two discussed alternatives is defined as:

$$[T] = \begin{bmatrix} [T]_{jj} & [T]_{pj} \\ [T]_{jp} & [T]_{pp} \end{bmatrix} \tag{A.3a}$$

$$[T]^{ALT1}_{pp} = \begin{bmatrix} 1 & 0 & 0 & 0 & -49 & 22.5 & -1102 \\ 0 & 1 & 0 & 0 & 0 & 0 & 0 \\ 0 & 0 & 1 & 52.57 & 0 & 0 & 0 \\ 0 & 0 & 0 & 1 & 0 & 0 & 0 \\ 0 & 0 & 0 & 0 & 1 & 0 & 52.57 \\ 0 & 0 & 0 & 0 & 0 & 1 & 0 \\ 0 & 0 & 0 & 0 & 0 & 0 & 1 \end{bmatrix} ; [T]^{ALT2}_{pp} = \begin{bmatrix} 1 & 0 & 0 & 0 & -49 & 22.5 & 0 \\ 0 & 1 & 0 & 0 & 0 & 0 & 0 \\ 0 & 0 & 1 & 52.57 & 0 & 0 & 0 \\ 0 & 0 & 0 & 1 & 0 & 0 & 0 \\ 0 & 0 & 0 & 0 & 1 & 0 & 0 \\ 0 & 0 & 0 & 0 & 0 & 1 & 0 \\ 0 & 0 & 0 & 0 & 0 & 0 & 1 \end{bmatrix} \tag{A.3b,c}$$

A fixed end is located at node j and all the corresponding degrees of freedom are locked, i.e. all the corresponding columns and rows are deleted from the final matrix. As a consequence, the elastic stiffness matrix referred to the global system has a range of 7 and it is thus equal to:

$$[K]^{E,g} = [T][K]^{E,l}[T]^T \tag{A.4a}$$

By applying the two alternatives, the result is:

$$[K]^{E,gALT1}_{pp} = \begin{bmatrix} 5.2 \cdot 10^4 & 0 & 0 & 0 & -2.5 \cdot 10^6 & 1.1 \cdot 10^6 & -5.6 \cdot 10^7 \\ 0 & 9.3 \cdot 10^1 & 0 & 0 & 0 & -9.3 \cdot 10^4 & 0 \\ 0 & 0 & 2.7 \cdot 10^2 & 1.4 \cdot 10^4 & 2.7 \cdot 10^5 & 0 & 1.4 \cdot 10^7 \\ 0 & 0 & 1.4 \cdot 10^4 & 9.4 \cdot 10^5 & 1.4 \cdot 10^4 & 0 & 9.2 \cdot 10^8 \\ -2.5 \cdot 10^6 & 0 & 2.7 \cdot 10^5 & 1.4 \cdot 10^7 & 4.9 \cdot 10^8 & -5.6 \cdot 10^7 & 2.2 \cdot 10^{10} \\ 1.1 \cdot 10^6 & -9.3 \cdot 10^4 & 0 & 0 & -5.6 \cdot 10^7 & 1.5 \cdot 10^8 & -1.3 \cdot 10^9 \\ -5.6 \cdot 10^7 & 0 & 1.4 \cdot 10^7 & 9.2 \cdot 10^8 & 2.2 \cdot 10^{10} & -1.3 \cdot 10^9 & 1.3 \cdot 10^{12} \end{bmatrix} \tag{A.4b}$$

$$[K]_{pp}^{E,g\,ALT2} = \begin{bmatrix} 5.2 \cdot 10^4 & 0 & 0 & 0 & -2.5 \cdot 10^6 & 1.1 \cdot 10^6 & 0 \\ 0 & 9.3 \cdot 10^1 & 0 & 0 & 0 & -9.3 \cdot 10^4 & 0 \\ 0 & 0 & 2.7 \cdot 10^2 & 1.4 \cdot 10^4 & 2.7 \cdot 10^5 & 0 & 0 \\ 0 & 0 & 1.4 \cdot 10^4 & 9.4 \cdot 10^5 & 1.4 \cdot 10^7 & 0 & 1.6 \cdot 10^8 \\ -2.5 \cdot 10^6 & 0 & 2.7 \cdot 10^5 & 1.4 \cdot 10^7 & 4.9 \cdot 10^8 & -5.6 \cdot 10^7 & 0 \\ 1.1 \cdot 10^6 & -9.3 \cdot 10^4 & 0 & 0 & -5.6 \cdot 10^7 & 1.5 \cdot 10^8 & 0 \\ 0 & 0 & 0 & 1.6 \cdot 10^8 & 0 & 0 & 2.2 \cdot 10^{11} \end{bmatrix} \tag{A.4c}$$

The external load vector in the global reference system contains only one term, i.e. the one corresponding to the applied axial force (-1000 N), different from zero.

The global displacement can be evaluated as:

$$\{u\}_p = \left([K]_{pp}^{E,g}\right)^{-1} \{F\}_p \tag{A.5a}$$

$$\{u\}_p^{ALT1} = \begin{bmatrix} 8.8 \cdot 10^{-5} & -7.1 \cdot 10^{-4} & -1.3 \cdot 10^{-3} & 1.5 \cdot 10^{-5} & 1.5 \cdot 10^{-6} & -7.1 \cdot 10^{-7} & -1.8 \cdot 10^{-8} \\ -7.1 \cdot 10^{-4} & 4.3 \cdot 10^{-2} & -7.8 \cdot 10^{-17} & 1.8 \cdot 10^{-18} & 1.1 \cdot 10^{-19} & 3.2 \cdot 10^{-5} & 2.4 \cdot 10^{-21} \\ -1.3 \cdot 10^{-3} & 6.0 \cdot 10^{-19} & 5.4 \cdot 10^{-2} & -7.4 \cdot 10^{-4} & -3.9 \cdot 10^{-5} & 6.0 \cdot 10^{-22} & 5.4 \cdot 10^{-7} \\ 1.5 \cdot 10^{-5} & 1.5 \cdot 10^{-20} & -7.4 \cdot 10^{-4} & 1.4 \cdot 10^{-5} & 5.4 \cdot 10^{-7} & 1.5 \cdot 10^{-23} & -1.0 \cdot 10^{-8} \\ 1.5 \cdot 10^{-6} & -4.7 \cdot 10^{-22} & -3.9 \cdot 10^{-5} & 5.4 \cdot 10^{-7} & 4.4 \cdot 10^{-8} & -4.7 \cdot 10^{-25} & -6.2 \cdot 10^{-10} \\ -7.1 \cdot 10^{-7} & 3.2 \cdot 10^{-5} & -1.2 \cdot 10^{-19} & 2.3 \cdot 10^{-21} & 1.1 \cdot 10^{-22} & 3.2 \cdot 10^{-8} & -2.1 \cdot 10^{-24} \\ -1.8 \cdot 10^{-8} & -1.8 \cdot 10^{-23} & 5.4 \cdot 10^{-7} & -1.0 \cdot 10^{-8} & -6.2 \cdot 10^{-10} & -1.8 \cdot 10^{-26} & 1.2 \cdot 10^{-11} \end{bmatrix} \begin{Bmatrix} -1000 \\ 0 \\ 0 \\ 0 \\ 0 \\ 0 \\ 0 \end{Bmatrix} = \begin{Bmatrix} -0.088 \\ 0.715 \\ 1.336 \\ -0.015 \\ -0.0015 \\ 0.00072 \\ 1.7 \cdot 10^{-5} \end{Bmatrix} \tag{A.5b}$$

$$\{u\}_p^{ALT2} = \begin{bmatrix} 6.2 \cdot 10^{-5} & -7.1 \cdot 10^{-4} & -5.4 \cdot 10^{-4} & 2.9 \cdot 10^{-20} & 5.4 \cdot 10^{-7} & -7.1 \cdot 10^{-7} & -7.1 \cdot 10^{-25} \\ -7.1 \cdot 10^{-4} & 4.3 \cdot 10^{-2} & 1.3 \cdot 10^{-17} & 3.2 \cdot 10^{-19} & -7.0 \cdot 10^{-21} & 3.2 \cdot 10^{-5} & 5.8 \cdot 10^{-24} \\ -5.4 \cdot 10^{-4} & 0 & 5.4 \cdot 10^{-2} & -7.4 \cdot 10^{-4} & -1.1 \cdot 10^{-5} & 0 & 5.4 \cdot 10^{-7} \\ 0 & 0 & -7.4 \cdot 10^{-4} & 1.4 \cdot 10^{-5} & 0 & 0 & -1.0 \cdot 10^{-8} \\ 5.4 \cdot 10^{-7} & 0 & -1.1 \cdot 10^{-5} & 3.3 \cdot 10^{-22} & 1.1 \cdot 10^{-8} & 0 & -2.3 \cdot 10^{-25} \\ -7.1 \cdot 10^{-7} & 3.2 \cdot 10^{-5} & 4.0 \cdot 10^{-21} & -3.5 \cdot 10^{-23} & -5.2 \cdot 10^{-24} & 3.2 \cdot 10^{-8} & -2.0 \cdot 10^{-26} \\ 0 & 0 & 5.4 \cdot 10^{-7} & -1.0 \cdot 10^{-8} & 0 & 0 & 1.2 \cdot 10^{-11} \end{bmatrix} \begin{Bmatrix} -1000 \\ 0 \\ 0 \\ 0 \\ 0 \\ 0 \\ 0 \end{Bmatrix} = \begin{Bmatrix} -0.019 \\ 0.715 \\ 0.537 \\ 0 \\ -0.00054 \\ 0.00072 \\ 0 \end{Bmatrix} \tag{A.5c}$$

It should be noted that, the generalised displacements associated with the two alternatives are practically coincident with the corresponding ones reported in Table 5, despite the use of a single finite element. Finally, the internal forces have been appraised from the displacement vector and referred to the local reference system by using the complete algebraic linear system (range 14). For the two alternatives, the result is:

$$\{F\}^l = [K]^{E,l} \left([T]\{u\}\right) \tag{A.6a}$$

$$\{F\}^{l\,ALT1} = [K]^{E,l} \begin{Bmatrix} 0 \\ 0 \\ 0 \\ 0 \\ 0 \\ 0 \\ 0 \\ -0.0193 \\ 0.715 \\ 0.537 \\ -0.0151 \\ -0.00054 \\ 0.00072 \\ -0.000018 \end{Bmatrix} = \begin{Bmatrix} 1000 \\ 0 \\ 0 \\ 0 \\ 49000 \\ -22260 \\ -555858 \\ -1000 \\ 0 \\ 0 \\ 0 \\ -49000 \\ 22260 \\ 1485190 \end{Bmatrix}; \qquad \{F\}^{l\,ALT2} = [K]^{E,l} \begin{Bmatrix} 0 \\ 0 \\ 0 \\ 0 \\ 0 \\ 0 \\ 0 \\ -0.0193 \\ 0.715 \\ 0.537 \\ 0 \\ -0.00054 \\ 0.00072 \\ 0 \end{Bmatrix} = \begin{Bmatrix} 1000 \\ 0 \\ 0 \\ 0 \\ 49000 \\ -22260 \\ 0 \\ -1000 \\ 0 \\ 0 \\ 0 \\ -49000 \\ 22260 \\ 0 \end{Bmatrix}; \tag{A.6b, c}$$

These data stress confirm a very important result: with Alt. 2 there is no bimoment (terms 7 and 14 of $\{F\}^l$ vectors) associated with the axial force (Vlasov's first theorem). Conversely, Alt. 1 leads to a bimoment value (555 kN mm^2) at the fixed end that is approximately 22% lower than the theoretical one (Table 5). This discrepancy is due to the use of a single finite element, which is not enough to describe the effective bimoment distribution. It is worth noting that by adding more FE beams (at least four) the end bimoment tends towards the right value.

References

[1] C. Bernuzzi, E. Bertinotti, M. Simoncelli, Structural analysis of built-up members with angles, J. Appl. Eng. Sci. 18 (3) (2020) 443–457.

[2] J.R. Maguire, L.H. Teh, G.C. Clifton, J.B.P. Lim, Residual capacity of cold-formed steel rack uprights following stomping during rocking, J. Construct. Steel Res. 159 (2019) 189–197.

[3] S.P. Timoshenko, J.M. Gere, Theory of Elastic Stability, second ed., McGraw Hill New-York, 1961.

[4] Vlasov V. Z., Thin Walled Elastic Beams, second Ed., Israel Program for Scientific Transactions, Jerusalem, Israel, 1961.

[5] S.U. Benscoter, P. Calif, A theory od torsion bending for multicell beams, J. Appl. Mech. 211 (1954) 25–34.

[6] H. Shakourzadeh, Y.Q. Guo, J.-L. Batoz, A torsion bending element for thin-walled beams with open and closed cross section, Comput. Struct. 55 (6) (1995) 1045–1054.

[7] W.F. Chen, T. Atzuta, Theory of Beam–Columns: 2 Space Behaviour and Design, McGraw Hill, 1977.

[8] P. Di Re, D. Addessi, Computational enhancement of a mixed 3D beam finite element with warping and damage, J. Appl. Comput. Mech. 8 (1) (2022) 260–281.

[9] K.M. Hsiao, W.Y. Lin, A co-rotational formulation for thin-walled beams with mono-symmetric open sections, Comput. Methods Appl. Mech. Engrg. 190 (8) (2000) 1163–1185.

[10] G. Turkalj, J. Brnic, J. Prpic-Orsic, Large rotation analysis of elastic thin-walled beam-type structures using ESA approach, Comput. Struct. 81 (18–19) (2003) 1851–1864.

[11] S. Liu, W.L. Gao, R. Ziemian, Improved line-element formulations for the stability analysis of arbitrarily shaped open-section beam–columns, Thin Walled Struct. 144 (2019) 106290.

[12] A. Genoese, A. Genoese, A. Bilotta, G. Garcea, A geometrically exact beam model with non-uniform warping coherently derived from the saint venant rod, Eng. Struct. 68 (1) (2014) 33–46.

[13] D. Addessi, P. Di Re, G. Cimarello, Enriched beam finite element models with torsion and shear warping for the analysis of thin-walled structures, Thin Walled Struct. 159 (2021) 107259.

[14] D. Camotim, C. Basaglia, N. Silvestre, GBT buckling analysis of thin-walled steel frames: A state-of-the-art report, Thin Walled Struct. 48 (10–11) (2010) 726–743.

[15] SeismoStruct software, 2023, https://seismosoft.com/. (Accessed 2023).

[16] ABAQUS software, 2023, https://www.3ds.com/it/prodotti-e-servizi/simulia/prodotti/abaqus/. (Accessed 2023).

[17] Midas GEN software, 2023, https://www.midasstructure.com/en/. (Accessed 2023).

[18] Consteel software, 2023, https://consteelsoftware.com/. (Accessed 2023).

[19] Ansys, 2023, https://www.ansys.com/it-it. (Accessed 2023).

[20] Mastan2 v5.1, 2023, https://www.mastan2.com/. (Accessed 2023).

[21] A. Prokić, R. Mandić, M. Vojinć-Purčar, Influence of bimoment on the torsional and flexural–torsional elastic stability of thin-walled beams, Thin Walled Struct. 59 (2015) 22–30.

[22] CEN, EN1993, Eurocode 3 - Design of Steel Structures - Part 1-1: General Rules and Rules for Buildings, European Committee For Standardization CEN Brussels, 2005.

[23] AISI S100-16, North American Standard for Cold-Formed Steel Structural Framing, American Iron and Steel Institute, 2020.

[24] CEN, PrEN1993, Eurocode 3 - Design of Steel Structures - Part 1-1: Design of Steel Structures, General Rules and Rules for Buildings, European Committee For Standardization CEN Brussels, 2022.

[25] G.J. Hancock, Portal frames composed of cold-formed channel and zed-sections, in: R. Narayanan (Ed.), Steel Framed Structures - Stability and Strength, Elsevier Applied Science. Publishers, London, 1985, pp. 241–275.

[26] G. Gabbianelli, A. Kanyilmaz, C. Bernuzzi, C.A. Castiglioni, A combined experimental numerical study on unbraced pallet rack under pushover loads, Ingegn. Sismica 34 (1) (2017) 18–38.

[27] CEN, Eurocode 3 - Design of Steel Structures - Part 1-3: Design of Cold Formed Members, European Committee For Standardization CEN Brussels, 2005.

[28] S. Liu, R. Ziemian, L. Chen, S. Chan, Bifurcation and large-deflection analyses of thin-walled beam–columns with non-symmetric open-sections, Thin Walled Struct. 132 (2018) 287–301.

[29] A. Kanyilmaz, C.A. Castiglioni, G. Brambilla, G.P. Chiarelli, Experimental assessment of the seismic behavior of unbraced steel storage pallet racks, Thin Walled Struct. 108 (2016) 391–405.

[30] CEN, EN15512 - Steel Static Storage Systems — Adjustable Pallet Racking Systems — Principles for Structural Design, CEN European Committee for Standardization, 2009.

[31] A. Carpinteri, G. Lacidogna, B. Montrucchio, S. Cammarano, The effect of the warping deformation on the structural behaviour of thin-walled open section shear walls, Thin Walled Struct. 84 (2014) 335–343.
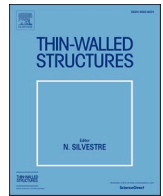
Corrigendum

Corrigendum to 'the transformation matrix in the 7DOFs beam formulation'

Claudio Bernuzzi, Marco Simoncelli [*]

Department of Architecture, Built Environment and Construction Engineering, Politecnico di Milano, Italy

A B S T R A C T

None.

The authors regret that the Ref. [21] in the published version has incorrect volume number. The Ref. [21] should read as follows:

The authors would like to apologize for any inconvenience caused.

Declaration of Competing Interest

None.

Reference

[21] A. Prokić, R. Mandić, M. Vojinć-Purčar, Influence of bimoment on the torsional and flexural–torsional elastic stability of thin-walled beams, Thin Walled Struct. 89 (2015) 25–30, https://doi.org/10.1016/j.tws.2014.12.005.